bioRxiv preprint doi: https://doi.org/10.1101/2021.02.16.431453; this version posted February 17, 2021. The copyright holder for this preprint (which was not certified by peer review) is the author/funder, who has granted bioRxiv a license to display the preprint in perpetuity. It is made available under aCC-BY 4.0 International license.

1 # Col6a1⁺/CD201⁺ telocytes regulate intestinal morphogenesis and homeostasis

2

3 Maria-Theodora Melissari[1,a], Ana Henriques[1,a,b], Christos Tzaferis[2], Alejandro
4 Prados[2], Michalis E. Sarris[1], Panagiotis Chouvardas[2,3,4], Sofia Grammenoudi[1], George
5 Kollias[2,5] and Vasiliki Koliaraki[1]

6

7 [1]Institute for Fundamental Biomedical Research, Biomedical Sciences Research
8 Center (B.S.R.C.) "Alexander Fleming", Vari, 16672, Greece; [2]Institute for
9 Bioinnovation, Biomedical Sciences Research Center (B.S.R.C.) "Alexander
10 Fleming", Vari, 16672, Greece; [3]Department of Medical Oncology, Inselspital, Bern
11 University Hospital, University of Bern, Switzerland; [4]Department for BioMedical
12 Research, University of Bern, Bern, Switzerland; [5]Department of Physiology, Medical
13 School, National and Kapodistrian University of Athens, Athens, 11527, Greece

14

15 [a]M.T.M and A.H. contributed equally to this work.

16 [b]Present address: Institute for Research in Biomedicine (IRB Barcelona), The
17 Barcelona Institute of Science and Technology, Barcelona, Spain.

18

19 **Correspondence:**

20 Vasiliki Koliaraki,

21 E-mail: koliaraki@fleming.gr

22

23

24

bioRxiv preprint doi: https://doi.org/10.1101/2021.02.16.431453; this version posted February 17, 2021. The copyright holder for this preprint (which was not certified by peer review) is the author/funder, who has granted bioRxiv a license to display the preprint in perpetuity. It is made available under aCC-BY 4.0 International license.

25 **Abstract**

26 Intestinal mesenchymal cells encompass multiple subsets, whose origins, functions,
27 and pathophysiological importance are still not clear. Here, we used the *Col6a1*^{Cre}
28 mouse, which targets telocytes and perivascular cells that can be further distinguished
29 by the combination of the CD201, PDGFRα and αSMA markers. Lineage tracing
30 revealed that telocytes originate from mesenchymal aggregates and are crucial for
31 intestinal morphogenesis and patterning. Cell depletion experiments showed that
32 Col6a1^{+}/CD201^{+} telocytes regulate homeostatic enteroendocrine cell differentiation
33 and epithelial proliferation. During acute colitis, they expressed an inflammatory and
34 extracellular matrix remodeling gene signature, but they also retained their properties
35 and topology. Notably, both in homeostasis and tissue regeneration, they were
36 dispensable for normal organ architecture, as they were replaced by CD34^{+}
37 mesenchymal cells, providing thus evidence for the plasticity potential of distinct
38 mesenchymal populations in the intestine. Therefore, our results provide a
39 comprehensive analysis of the identities, origin, and functional significance of colonic
40 *Col6a1*$^{Cre+}$ telocytes.

41

42

43

bioRxiv preprint doi: https://doi.org/10.1101/2021.02.16.431453; this version posted February 17, 2021. The copyright holder for this preprint (which was not certified by peer review) is the author/funder, who has granted bioRxiv a license to display the preprint in perpetuity. It is made available under aCC-BY 4.0 International license.

44 **Introduction**

45 The mammalian intestine is characterized by a unique architecture, which ensures
46 both efficient nutrient and water absorption and rapid self-renewal of the intestinal
47 epithelium. Self-renewal is mediated by Lgr5^{+} multi-potent crypt-base stem cells
48 (CBCs) that progressively give rise to transit amplifying (TA) progenitor cells and
49 differentiated epithelial cell populations with specific absorptive or secretive
50 functions [1, 2]. The tight regulation of this architectural organization is mediated by
51 a gradient of factors produced both by epithelial and stromal cells. Among stromal
52 cells, intestinal mesenchymal cells (IMCs) have emerged as an important cell type for
53 the development and homeostasis of the intestine, by providing both structural support
54 and regulatory elements [3]. Of particular interest is their contribution to the
55 maintenance of the stem cell niche via the production of soluble mediators [4].
56 Notably, in the absence of epithelial Wnts, production of stromal Wnts is sufficient
57 for the maintenance of epithelial proliferation, while depletion of Foxl1^{+} telocytes or
58 Grem1^{+} trophocytes, which produce niche-supporting factors led to the disruption of
59 the intestinal structure [5-7]. Additionally, BMP production by villous mesenchymal
60 cells inhibits proliferation and favors epithelial cell differentiation, which ensures
61 epithelial homeostasis and supports specialized epithelial functions [8, 9]. The
62 production of such signals is believed to be induced and maintained via the reciprocal
63 communication with epithelial cells. This has been convincingly shown during
64 embryonic development, where PDGF and Hh proteins secreted from the endodermal
65 epithelium act on the underlying mesenchyme to induce the formation of PDGFRα^{+}
66 aggregates, which express BMPs and regulate vilification of the intestine [10].

67 Beyond their homeostatic functions, intestinal fibroblasts contribute significantly to
68 tissue damage and inflammation. During such conditions, resident fibroblastic cells

bioRxiv preprint doi: https://doi.org/10.1101/2021.02.16.431453; this version posted February 17, 2021. The copyright holder for this preprint (which was not certified by peer review) is the author/funder, who has granted bioRxiv a license to display the preprint in perpetuity. It is made available under aCC-BY 4.0 International license.

69 are activated to produce pro-inflammatory cytokines and chemokines, angiogenic
70 factors, as well as extracellular matrix (ECM) components and remodeling enzymes
71 to facilitate acute inflammatory responses. Deregulation of these processes or chronic
72 injury can lead to chronic inflammatory disorders and fibrosis [11]. Indeed, recent
73 data point to an important role of the microenvironment in shaping cellular programs
74 and driving epithelial regeneration, as fibroblast-specific deletion of the Wnt regulator
75 porcupine (Porcn) or R-spondin 3 led to severely impaired intestinal regeneration [12,
76 13].

77 Until recently, mesenchymal cells in the intestine, although known to constitute a
78 group of cell types, were frequently studied as one, mainly due to difficulties in
79 marking, isolating and genetically targeting specific populations. However, recent
80 single-cell transcriptomic analyses of the normal mouse and human intestine revealed
81 the underappreciated extent of mesenchymal heterogeneity and identified several
82 fibroblast subsets with distinct expression profiles and functions [4, 7, 14-16].
83 However, their origin and spatial organization, as well as the mechanisms through
84 which distinct subsets coordinate signaling gradients along the crypt-villus axis in
85 homeostasis and disease remain elusive. The use of specific markers and Cre-
86 expressing mouse lines have begun to provide such information and are crucial for
87 addressing these issues. Examples include CD34, Foxl1, PDGFRα and Gli1 positive
88 IMCs, which act as critical regulators of the intestinal stem cell niche through their
89 production of Wnts, R-spondins and Gremlin 1, although they are not strictly
90 restricted to single cell types [6, 7, 12, 13, 17, 18]. Lgr5^{+} villous tip telocytes were
91 also recently shown to regulate epithelial villus tip gene expression programs [19].
92 Single-cell analysis of the inflamed intestine has further highlighted the prominent
93 pro-inflammatory activation of fibroblasts [14, 15, 20]. Notably, activated fibroblasts

bioRxiv preprint doi: https://doi.org/10.1101/2021.02.16.431453; this version posted February 17, 2021. The copyright holder for this preprint (which was not certified by peer review) is the author/funder, who has granted bioRxiv a license to display the preprint in perpetuity. It is made available under aCC-BY 4.0 International license.

94 along with immune cells were associated with resistance to anti-TNF therapy,
95 indicating their potential utility in patient diagnosis, stratification and therapeutic
96 decisions [15, 20].
97 We have previously shown that the *Col6a1*^{Cre} transgenic mouse targets a fraction of
98 mesenchymal cells in the intestine and that NFκB signaling in this subset uniquely
99 protects against colitis and colitis-associated cancer [21]. In this study, transcriptomic,
100 imaging and functional analysis of the cells targeted by the *Col6a1*^{Cre} mouse revealed
101 preferential targeting of colonic telocytes/subepithelial myofibroblasts (SEMFs) and
102 perivascular cells, which can be further described by the use of specific markers.
103 Using lineage tracing and cell depletion approaches we have further identified their
104 origin from mesenchymal clusters during embryogenesis, as well as their functional
105 significance in development and adulthood. Notably, both in normal conditions and
106 during tissue regeneration, CD34^{+} IMCs could compensate for the loss of colonic
107 *Col6a1*$^{Cre+}$ telocytes, revealing the plasticity of IMCs towards organ homeostasis.
108
109 **Results**

110 **The *Col6a1*^{Cre} mouse targets CD34^{-} mesenchymal cells in the intestine**

111 We have shown in the past that the *Col6a1*^{Cre} transgenic mouse targets a fraction of
112 mesenchymal cells in the intestine [21]. To define its specificity for distinct
113 mesenchymal subsets, we crossed *Col6a1*^{Cre} mice with a TdTomato-to-GFP
114 replacement (mTmG) reporter strain (*Col6a1*^{mTmG}) and after exclusion of immune,
115 endothelial, erythroid and epithelial cells using the lineage negative (Lin^{-}) markers
116 CD45, CD31, Ter119 and CD326 (EpCAM), we isolated *Col6a1*-GFP^{+} and *Col6a1*-
117 GFP^{-} IMCs by FACS sorting (Figure 1A). As previously reported, the *Col6a1*^{Cre}
118 mouse does not target Lin^{+} cells [21]. We then performed 3' mRNA sequencing of the

bioRxiv preprint doi: https://doi.org/10.1101/2021.02.16.431453; this version posted February 17, 2021. The copyright holder for this preprint (which was not certified by peer review) is the author/funder, who has granted bioRxiv a license to display the preprint in perpetuity. It is made available under aCC-BY 4.0 International license.

119 Lin$^-$GFP$^+$ IMCs (GC), Lin$^-$Tomato$^+$ IMCs (TC) and the initial unsorted cells (UC).
120 Gene Ontology (GO) analysis of the upregulated genes in the GC versus the TC
121 and/or UC cells revealed enrichment in biological processes related to epithelial cell
122 proliferation and differentiation, as well as regulation of vasoconstriction and blood
123 pressure (Figure 1B). Enriched genes associated with epithelial differentiation
124 included Bmps (*Bmp3*, *Bmp7*, *Bmp2*, *Bmp5*), *Wnt5a,* the Wnt inhibitor *Wif1* and
125 genes related to the differentiation of epithelial cells (e.g. *Fgf9*) [8]. Conversely, the
126 TC population expressed genes associated with the maintenance of the stem cell
127 niche, such as *Grem1*, *Wnt2* and *Nog* [7, 17] (Figure 1B).
128 A similar cell sorting and sequencing approach was also performed for the small
129 intestine, where two populations of GFP$^+$ cells were identified, a GFP^{hi} (GIH) and a
130 GFP^{lo} (GIL) population, each accounting for 23% and 29% of the Lin$^-$ population,
131 respectively (Figure supplement 1A). Analysis of the genes identified in the colon
132 showed that GIH cells were also enriched in genes related to epithelial differentiation
133 and blood vessel function, while GFP^{lo} (GIL) cells were similar to the GFP$^-$
134 population (Figure supplement 1B). The presence of GFP^{lo} cells in the small intestine
135 indicates a GFP$^+$ cell population with potentially different cellular properties [22], and
136 could represent a distinct cell subset, an intermediate state between GFP$^-$ and GFP$^+$
137 cells or the result of non-specific recombination. These results suggest that *Col6a1*$^{Cre+}$
138 cells have distinct homeostatic functions, potentially associated with different
139 topologies along the colonic crypt length and the crypt/villous axis in the small
140 intestine.
141 Interestingly, one of the genes enriched in the GFP$^-$ samples in both the small
142 intestine and colon was *Cd34* (Figure 1B). Stzepourginski et al. [17] described a
143 broad population of PDPN$^+$CD34$^+$ cells, which are located at the bottom of the crypts,

bioRxiv preprint doi: https://doi.org/10.1101/2021.02.16.431453; this version posted February 17, 2021. The copyright holder for this preprint (which was not certified by peer review) is the author/funder, who has granted bioRxiv a license to display the preprint in perpetuity. It is made available under aCC-BY 4.0 International license.

144 express Gremlin1, Wnt2b and R-spondin, and play a role in stem cell maintenance.
145 FACS analysis and immunohistochemistry showed that indeed the majority of GFP^{+}
146 cells in the colon and GFP^{hi} in the small intestine were CD34 negative and further
147 indicated a preferential subepithelial localization for GFP^{+} cells outside the bottom of
148 the crypts (Figure 1C-D and Figure supplement 1C-D). Consistent with this data, co-
149 culture of either GFP^{+} or GFP^{-} IMCs with intestinal organoids showed that GFP^{+} cells
150 were less potent than GFP^{-} cells in supporting the growth of epithelial organoids in
151 the absence or presence of R-spondin 1 (Figure 1E-F). Comparison of the gene
152 signature of mesenchymal subsets from the recently published single-cell RNA
153 sequencing of the mouse colon by Kinchen et al., [14] and the gene expression profile
154 of GFP^{+} cells revealed an association with the Str2 cluster (Figure 1G-H).
155 Importantly, this cluster appears to be the highest conserved between mice and
156 humans [14]. These results show that the *Col6a1*^{Cre} mouse targets predominantly
157 CD34^{-} mesenchymal cells outside the bottom of the intestinal crypt, rendering it ideal
158 for the functional characterization of these cells.
159

160 **Colonic *Col6a1*^{Cre}-GFP^{+} cells are CD201 positive and include predominantly**
161 **telocytes/SEMFs**

162 We next searched our sequencing data for markers that could be used to detect, isolate
163 and study *Col6a1*^{Cre}-GFP^{+} cells. We found that GFP^{+} cells express higher levels of
164 CD201 (Procr or EPCR), which was further verified by immunohistochemistry
165 (Figure 2A). FACS analysis indeed showed that 67% and 48% of the Lin^{-}GFP^{+}
166 population in the colon and Lin^{-}GFP^{hi} in the small intestine were CD201^{+},
167 respectively (Figure 2B and Figure supplement 1E). It should be noted that CD201 is
168 also expressed by endothelial cells, which are excluded as Lin^{-} in our analysis. Since

bioRxiv preprint doi: https://doi.org/10.1101/2021.02.16.431453; this version posted February 17, 2021. The copyright holder for this preprint (which was not certified by peer review) is the author/funder, who has granted bioRxiv a license to display the preprint in perpetuity. It is made available under aCC-BY 4.0 International license.

169 not all GFP^+ cells express CD201, we also isolated $Lin^-GFP^+CD201^+$ and Lin^-
170 GFP^+CD201^- cells from the colon by FACS sorting. qPCR analysis showed that
171 GFP^+CD201^+, but not GFP^+CD201^- cells, expressed genes related both to the
172 regulation of blood vessel function and epithelial cell differentiation, similar to GFP^+
173 cells (Figure 2C). These results suggest that the remaining *Col6a1*$^{Cre+}$$CD201^-$ cells
174 either have another yet unknown role in the intestine or are the result of non-specific
175 targeting by the *Col6a1*^{Cre} mouse.
176 Combination of the CD201 and CD34 markers along with Lin^- expression was able to
177 distinguish between the two distinct intestinal mesenchymal populations (Figure 2D
178 and Figure supplement 2A). Additional co-staining with PDGFRα and αSMA
179 revealed the presence of multiple subsets within $CD201^+$ cells, including $PDGFR\alpha^{hi}$-
180 $\alpha SMA^{lo/-}$ (66%), $PDGFR\alpha^{lo}$-$\alpha SMA^{lo/-}$ (25%) and $PDGFR\alpha^-\alpha SMA^{hi}$ cells (3%) (Figure
181 2D and Figure supplement 2B-D). $CD34^+$ cells were mainly $PDGFR\alpha^{lo/-}$ and only a
182 limited number expressed αSMA, in line with recent reports [7, 17] (Figure 2D).
183 $GFP^+PDGFR\alpha^-\alpha SMA^{hi}$ cells were found around blood vessels and were most possibly
184 pericytes (Figure 2E and Figure supplement 2D), as also indicated by qPCR analysis
185 (Figure supplement 2E) and previous results [4, 23]. $GFP^+PDGFR\alpha^{hi}\alpha SMA^{lo/-}$ were
186 long thin cells in a subepithelial location found both clustered at the top of the colonic
187 crypts and individually along the crypt's length, corresponding to telocytes or
188 subepithelial myofibroblast (SEMFs) (Figure 2F-H and Figure supplement 2C) [4, 7,
189 13, 19]. Indeed, GFP^+ cells expressed markers related to telocytes, including *Foxl1*,
190 *Bmp7, Wif1* and *Wnt5a* (Figure 1B and Figure supplement 2E). Finally,
191 $GFP^+PDGFR\alpha^{lo}$-$\alpha sma^{lo/-}$ cells appeared as flat cells with extended processes that
192 surround the colonic crypt (Figure 2F). FACS-based quantification of *Col6a1*^{Cre}-
193 GFP^+ cells in these subsets revealed targeting of almost all $CD201^+PDGFR\alpha^{hi}$

bioRxiv preprint doi: https://doi.org/10.1101/2021.02.16.431453; this version posted February 17, 2021. The copyright holder for this preprint (which was not certified by peer review) is the author/funder, who has granted bioRxiv a license to display the preprint in perpetuity. It is made available under aCC-BY 4.0 International license.

194 telocytes (96.7%) and one third of the PDGFRα^{lo} stroma (27.8%), including mainly
195 CD201^{+}PDGFRα^{lo} cells (77.8% versus 11.7% of CD34^{+}PDGFRα^{lo} cells) (Figure 2I).
196 Absence of Gremlin1 expression (Figure 1B) indicates that none of the latter include
197 trophocytes. The *Col6a1^{Cre}* mouse also targeted approximately 86% of
198 CD201^{+}αSMA^{hi} pericytes (Figure 2K). However, the apparent low abundancy of this
199 population suggests that expression of genes related to blood vessel function could be
200 also associated with the localization of *Col6a1^{Cre}*-GFP^{+} cells in close proximity to the
201 subepithelial capillary network, indicating thus a dual function for colonic
202 telocytes/SEMFs (Figure 2L). These results reveal the complexity of mesenchymal
203 cells surrounding the colonic crypt and provide a detailed characterization of their
204 markers and localization. They further suggest that the *Col6a1^{Cre}* mouse could be
205 used for the functional analysis of colonic telocytes/SEMFs.
206

207 **Telocytes/SEMFs originate from embryonic mesenchymal aggregates and**
208 **orchestrate intestinal morphogenesis**

209 To examine the origin of intestinal telocytes/SEMFs during embryonic organogenesis,
210 we analysed *Col6a1^{mTmG}* mice at different developmental stages. We found that GFP^{+}
211 cells were absent until E13.5 and started to appear at E14.5-E15.5 as aggregates
212 beneath the epithelial layer (Figure 3A). As villi became more elongated, GFP^{+} cells
213 extended toward the bottom of the crypts (Figure 3B). GFP^{+} aggregates expressed
214 PDGFRα, as shown by both confocal microscopy and FACS analysis, in line with
215 previous reports [24-26] (Figure 3A-B and 3D). Notably, similar GFP^{+} PDGFRα^{+}
216 aggregates were also detected in the developing colon (Figure 3A-B). FACS analysis
217 showed that the majority of GFP^{+} cells corresponded to 28% and 38.3% of PDGFRα^{hi}
218 cells at E16.5 and E18.5, respectively (Figure 3D and E). Contrary to adulthood, the

bioRxiv preprint doi: https://doi.org/10.1101/2021.02.16.431453; this version posted February 17, 2021. The copyright holder for this preprint (which was not certified by peer review) is the author/funder, who has granted bioRxiv a license to display the preprint in perpetuity. It is made available under aCC-BY 4.0 International license.

219 *Col6a1*^{Cre} mouse targeted a limited number of other mesenchymal populations,
220 including PDGFRα^{lo} and αSMA^{+} cells, which indicates its specificity for telocytes or
221 telocyte precursors during development (Figure 3D-E). It should be noted that CD34
222 was not expressed at this stage in agreement with previous reports [17]. CD201 was
223 broadly expressed, although it did include PDGFRα^{hi} cells also targeted by the
224 *Col6a1*^{Cre} mouse (Figure 3F). These results show that telocytes originate from
225 mesenchymal villous and colonic clusters and in combination with previous published
226 results [10] indicate that they acquire their identities during early organogenesis.
227 To define the physiological importance of these cells during intestinal embryonic
228 development, we employed the iDTR strain [27] in combination with the *Col6a1*^{mTmG}
229 mice (*Col6a1*^{DTR}). Administration of diptheria toxin (DT) in *Col6a1*^{DTR} mice at E14.5
230 and E15.5 and subsequent ex vivo culture of the embryonic intestine for 48 hours
231 resulted in depletion of *Col6a1*-GFP^{+} cells and a significant reduction in the number
232 of developing villi (Figure 3G-I, Figure supplement 3 and Supplementary Videos 1
233 and 2). Total and GFP^{-} villi were separately quantified in the *Col6a1*^{DTR} mice to take
234 into account potential inefficient or patchy deletion, while all villi appear to have
235 GFP^{+} clusters in the control mice (Figure 3I and Supplementary Videos 1 and 2).
236 Staining with PDGFRα and αSMA did not reveal major differences in their
237 expression patterns after GFP^{+} cell depletion, in agreement with the level of *Col6a1*^{Cre}
238 targeting at this stage (Figure 3C-E and 3H). These results provide direct proof for the
239 role of telocyte/SEMF precursors as orchestrators of intestinal morphogenesis and
240 patterning.
241

242 **Colonic *Col6a1*$^{Cre+}$ IMCs regulate homeostatic epithelial proliferation and**
243 **enteroendocrine cell differentiation**

bioRxiv preprint doi: https://doi.org/10.1101/2021.02.16.431453; this version posted February 17, 2021. The copyright holder for this preprint (which was not certified by peer review) is the author/funder, who has granted bioRxiv a license to display the preprint in perpetuity. It is made available under aCC-BY 4.0 International license.

244 To define the homeostatic roles of colonic *Col6a1*$^{Cre+}$ IMCs, we then depleted
245 *Col6a1*-GFP^{+} cells in 4-6-month-old *Col6a1*^{DTR} mice. Due to increased lethality upon
246 systemic DT injection, we performed local intrarectal DT administration, as shown in
247 Fig. 4A. Efficient, albeit not complete, depletion of GFP^{+} cells (75 % reduction) at the
248 last 3-4 cm of the colon was verified by confocal imaging and FACS analysis (Fig.
249 4B-C). Further analysis of the remaining GFP^{+} cells showed that although all
250 subtypes were depleted, there was a preferential loss of PDGFRα^{hi} cells and a
251 proportional increase in PDGFRα^{lo} cells (Fig. 4D). Accordingly, and consistent with
252 our previous data (Fig. 2), PDGFRα^{hi}CD201^{+} telocytes/SEMFs were reduced by 90%,
253 while PDGFRα^{lo} stromal cells were proportionally increased by 11%, and PDGFRα^{-}
254 cells remained largely unaltered (Fig. 4E-F). These results indicate that
255 telocytes/SEMFs is the mesenchymal subpopulation most efficiently depleted using
256 our approach. Histopathological examination of *Col6a1*^{DTR} mice showed that the
257 intestinal structure was normal following DT administration (Figure 4G).
258 Immunohistochemistry and/or qPCR analysis for the quantification of specific
259 intestinal epithelial subpopulations showed a reduction in enteroendocrine cell
260 differentiation upon GFP^{+} cell depletion, while stem cell maintenance, as well as the
261 differentiation of Tuft and Goblet cells was not affected (Figure 4H-I and Figure
262 supplement 4). Quantification of telocyte markers in these tissue samples showed a
263 reduction in *Bmp7* and *Wnt5a* expression levels, while the expression of most other
264 Bmps and *Foxl1* was not altered (Figure 4J). Notably, Bmp7, which forms
265 heterodimers with Bmp2 and Bmp4 was previously shown to be one of the factors
266 that is exclusively expressed by PDGFRα^{+} telocytes at the crypt-villous boundary of
267 the small intestine [7]. In addition, we also detected a defect in the distribution of
268 BrdU^{+} proliferating epithelial cells along the crypt axis, characterized by an increase

bioRxiv preprint doi: https://doi.org/10.1101/2021.02.16.431453; this version posted February 17, 2021. The copyright holder for this preprint (which was not certified by peer review) is the author/funder, who has granted bioRxiv a license to display the preprint in perpetuity. It is made available under aCC-BY 4.0 International license.

269 toward the top of the crypt, which could be associated with the role of BMPs in the
270 regulation of stem cells [28] (Figure 4K-L). These results show that colonic
271 *Col6a1*$^{Cre+}$ telocytes/SEMFs have distinct pathophysiological roles in epithelial cell
272 differentiation and proliferation, although they are largely dispensable for normal
273 tissue architecture and function.
274

275 **CD34^{+} mesenchymal cell plasticity compensates for the loss of *Col6a1*$^{Cre+}$ IMCs**

276 The similar expression levels of most BMPs in the *Col6a1*^{DTR} mice and its normal
277 tissue architecture indicated that other mesenchymal cell populations could mediate
278 some of the functions of *Col6a1*$^{Cre+}$ telocytes/SEMFs under these conditions. Indeed,
279 we found that colonic crypt tops in the *Col6a1*^{DTR} mice were populated by GFP^{-}
280 PDGFRα^{+}CD34^{+} cells, which however remained PDGFRα^{lo} (Figure 5A-B). CD34^{+}
281 cells in this area were also Ki67^{+}, indicating that these cells could proliferate and
282 occupy the space, where *Col6a1*$^{Cre+}$ telocytes were previously located (Figure 5C-D).
283 Interestingly, CD34^{+} cells in this area also expressed αSMA, a marker commonly
284 upregulated in response to fibroblast activation (Figure E-G). These results show that
285 following *Col6a1*$^{Cre+}$ telocyte/SEMF depletion, CD34^{+} cells become activated, they
286 proliferate and occupy the space at the top of the colonic crypts, partly compensating
287 for the loss of telocytes, providing thus evidence for mesenchymal plasticity in the
288 intestine.
289

290 **Topological and functional plasticity of mesenchymal cells during intestinal**
291 **regeneration**

292 To further explore the functions of *Col6a1*-GFP^{+} cells in non-homeostatic conditions,
293 we subjected *Col6a1*^{mTmG} mice to the DSS model of acute colitis and isolated Lin-

bioRxiv preprint doi: https://doi.org/10.1101/2021.02.16.431453; this version posted February 17, 2021. The copyright holder for this preprint (which was not certified by peer review) is the author/funder, who has granted bioRxiv a license to display the preprint in perpetuity. It is made available under aCC-BY 4.0 International license.

294 GFP$^+$ (GDS) and Lin-Tomato$^+$ (TDS) cells by FACS sorting, as previously described
295 (Figure 6A). Comparisons between GFP$^+$ and GFP$^-$ IMCs and the unsorted population
296 (UDS), as well as cells from untreated mice and subsequent Gene Ontology analysis
297 revealed that both GDS and TDS cells were enriched for functions related to
298 inflammatory/ immune responses (Figure 6B). GDS and TDS samples also showed
299 enrichment in genes related to epithelial proliferation/differentiation and blood vessel
300 function, similar to the homeostatic situation, suggesting that these cells, although
301 activated, retain their homeostatic properties and marker expression (Figure 6B and
302 Figure supplement 5A). FACS analysis of mesenchymal populations described in
303 Figure 2 verified their presence also during acute colitis, although CD201$^+$PDGFRα$^-$
304 αSMA^{hi} were increased in accordance with fibroblast activation (Figure supplement
305 5B-C). Confocal imaging further revealed that in sites of ulceration GFP$^+$ cells were
306 located in the upper part of the damaged area, indicating that they also retained their
307 topology (Figure 6C). This was further verified by comparisons with the recently
308 published single cell RNA-seq data by Kinchen et al., which confirmed that GDS
309 cells corresponded to the Str2 population [14] (Figure 6D).
310 Depletion of GFP$^+$ cells during DSS administration and evaluation of tissue
311 morphology 21 days after the initiation of the protocol showed similar
312 histopathological score to untreated mice, indicating normal regeneration of the
313 intestine (Figure 6E-H). Similar to homeostasis, GFP$^-$PDGFRα$^+$CD34$^+$ cells were
314 localized at the crypt tops, indicating the plasticity of CD34$^+$ cells and their ability to
315 differentiate to colonic *Col6a1*$^{Cre+}$ telocytes/SEMFs and support normal re-
316 epithelization of the colon (Figure 6I). Notably, at this late time-point, CD34$^+$ cells
317 were not αSMA$^+$, indicating their potential reversible activation following
318 *Col6a1Cre*$^+$ cell depletion (Fig. 6J). Therefore, these results further support the

bioRxiv preprint doi: https://doi.org/10.1101/2021.02.16.431453; this version posted February 17, 2021. The copyright holder for this preprint (which was not certified by peer review) is the author/funder, who has granted bioRxiv a license to display the preprint in perpetuity. It is made available under aCC-BY 4.0 International license.

319 plasticity of intestinal mesenchymal cells and suggest that reciprocal signals between
320 the epithelium and the underlying mesenchyme are more or equally important to
321 specialized cell types for intestinal regeneration.
322
323 **Discussion**

324 The importance of the mesenchymal stroma in the maintenance of intestinal structure
325 and function, as well as in the response to injury is now well-established [3, 4].
326 Opposing signaling gradients along the colonic crypt length and the crypt/villous axis
327 in the small intestine, including predominantly Wnts, BMPs, and their inhibitors, are
328 considered crucial for the maintenance of this morphology and the presence of
329 specialized mesenchymal cell types could explain this phenomenon [8]. Indeed,
330 several studies have described specific cell subsets that act as regulators of the stem
331 cell niche [6, 7, 13, 15-18]. Accordingly, although less studied, telocytes and specific
332 fibroblast subsets identified by sc-RNA sequencing analyses have been shown to
333 express BMPs and regulators of epithelial differentiation [6, 7, 14, 19, 29].
334 In this study, we focused on characterizing the identities, markers, origins and
335 functional significance of the latter in intestinal development, homeostasis and tissue
336 damage/regeneration using the *Col6a1*^{Cre} transgenic mouse [30]. To this end, we have
337 performed transcriptomic, FACS and imaging analysis of the cells targeted by the
338 *Col6a1*^{Cre} mouse strain. We also identified a novel extracellular marker, CD201, and
339 in combination with PDGFRα and αSMA we were able to show that the *Col6a1*^{Cre}
340 mice target almost all CD201^{+}PDGFRα^{hi}αSMA$^{lo/-}$ telocytes/SEMFs, around one third
341 of the PDGFRα^{lo} stroma, and specifically CD201^{+}PDGFRα^{lo} cells, as well as
342 perivascular cells that are CD201^{+}αSMA^{hi}. Among them, telocytes/SEMFs are the
343 only subpopulation targeted to its entirety, and it was shown to be present along the

bioRxiv preprint doi: https://doi.org/10.1101/2021.02.16.431453; this version posted February 17, 2021. The copyright holder for this preprint (which was not certified by peer review) is the author/funder, who has granted bioRxiv a license to display the preprint in perpetuity. It is made available under aCC-BY 4.0 International license.

344 colonic crypts, concentrating at their tops, in a similar fashion to the small intestine
345 [7]. In addition, they were in close proximity to the subepithelial capillary network,
346 indicating a potential dual role of telocytes/SEMFs in both epithelial and endothelial
347 cell function.
348 Little is known about the developmental origins of the different mesenchymal subsets,
349 including those identified through multiple single-cell analyses. Our results showed
350 that *Col6a1*$^{Cre+}$ telocytes originate from mesenchymal clusters during development
351 both in the small intestine and colon. These clusters have been previously shown to
352 emerge in the murine small intestine in waves after E13.5, they are PDGFRα^{+},
353 respond to Hedgehog signaling and express BMPs to regulate intestinal
354 morphogenesis [10, 24-26]. Similar mechanisms play an important role also in chick
355 intestinal development, where smooth muscle differentiation drives villi formation
356 through forces that generate localized pockets of high Shh, crucial for the expression
357 of mesenchymal cluster genes, such as PDGFRα and BMP4 [31, 32]. Deletion of
358 either PDGFα or PDGFRα in mice was shown to result in abnormal villi development
359 due to reduced mesenchymal proliferation [26]. Accordingly, inhibition of Hedgehog
360 signaling led to lack of cluster formation [24]. However, PDGFRα is broadly
361 expressed in the intestinal mesenchyme also during development, including both
362 high- and low- expressing cells, as we also show [26, 33]. Similarly, the Ptc1 receptor
363 and the downstream regulator Gli are not exclusive to mesenchymal aggregates
364 during development [24]. FoxL1 deletion also leads to a delay in vilification, but it is
365 expressed earlier at E12.5 and could target additional populations, as discussed below
366 [34]. In contrast, during development, the *Col6a1*^{Cre} mouse targets exclusively a
367 fraction of PDGFRα^{hi} cells located at the top of villi and colonic crypts. Therefore,
368 our functional analysis through cell depletion experiments provides proof for the

bioRxiv preprint doi: https://doi.org/10.1101/2021.02.16.431453; this version posted February 17, 2021. The copyright holder for this preprint (which was not certified by peer review) is the author/funder, who has granted bioRxiv a license to display the preprint in perpetuity. It is made available under aCC-BY 4.0 International license.

369 importance of mesenchymal cluster telocytes/telocyte precursors in intestinal
370 villification and patterning. Notably, a similar PDGFRA^{hi} population was also
371 recently described in the human developing intestine [35].
372 Interestingly, depletion of this population during homeostasis did not affect the
373 architecture and morphology of the colon, which is in agreement with the recent
374 depletion of Lgr5^{+} villous tip telocytes [19]. As we show, this apparent paradox can
375 be explained by the plasticity of CD34^{+} cells that are able to proliferate and occupy
376 the area, where *Col6a1*$^{Cre+}$/CD201^{+} telocytes/SEMFs were previously found.
377 However, several aspects of intestinal homeostasis were compromised, including the
378 expression levels of *Bmp7* and *Wnt5a*, the normal differentiation of enteroendocrine
379 cells and the distribution of proliferating cells along the crypt axis. Both the function
380 of enteroendocrine cells and the stemness of Lgr5^{+} cells have been previously shown
381 to be modulated by BMP signaling [9, 28], including Bmp7, which forms
382 heterodimers with Bmp2 and Bmp4 [35]. The exact CD34^{+} cell subset that displays
383 such plasticity is yet not known; however, Gremlin-1^{+} cells have been previously
384 shown to have stem cell potential in the intestine [36]. Notably, the phenotype of
385 *Col6a1*$^{Cre+}$/CD201^{+} telocyte/SEMF depletion is in contrast to FoxL1^{+} telocyte
386 deletion using a similar methodology. However, the *Foxl1*^{Cre} mouse has been shown
387 to target a heterogeneous mesenchymal cell population, including pericryptal
388 telocytes that express Gremlin-1 and myocytes [6, 13]. Although a small population,
389 Gremlin-1^{+} cells are crucial for intestinal homeostasis and structure, as recently
390 shown [7]. Therefore, our results, delineate the functional importance of *Col6a1*$^{Cre+}$
391 telocytes/SEMFs at the top of the colonic crypts, illustrate how they can affect
392 epithelial cell differentiation and proliferation and provide evidence for mesenchymal
393 plasticity towards tissue homeostasis.

bioRxiv preprint doi: https://doi.org/10.1101/2021.02.16.431453; this version posted February 17, 2021. The copyright holder for this preprint (which was not certified by peer review) is the author/funder, who has granted bioRxiv a license to display the preprint in perpetuity. It is made available under aCC-BY 4.0 International license.

394 Similar to homeostasis, *Col6a1*$^{Cre+}$ cell depletion during acute DSS colitis did not
395 affect inflammation and regeneration of the intestine, despite their inflammatory gene
396 signature and specific topology at the top of the ulcerated tissue and thus their
397 proximity to the regenerating epithelium. As we show, this is also associated with the
398 plasticity of CD34^{+} mesenchymal cells, which can replace *Col6a1*$^{Cre+}$
399 telocytes/SEMFs during the re-epithelization of the intestine, although the precise
400 identities of these cells remain unknown. These results further suggest that reciprocal
401 communication of the mesenchyme with the regenerating epithelium is crucial to
402 orchestrate tissue regeneration, although the specific molecular pathways are not yet
403 clear.
404 In conclusion, we have described the properties and identities of *Col6a1*$^{Cre+}$ colonic
405 telocytes/SEMFs, defined their origin from mesenchymal aggregates and identified
406 their role as orchestrators of intestinal morphogenesis and regulators of epithelial
407 homeostasis. We have further introduced the concept of mesenchymal plasticity both
408 during homeostasis and tissue repair at least towards telocyte differentiation. In the
409 future, it would be interesting to characterize the identities and role of these cells also
410 in other intestinal disorders, including cancer, and define the molecular mechanism
411 driving mesenchymal plasticity in homeostasis and disease.
412

bioRxiv preprint doi: https://doi.org/10.1101/2021.02.16.431453; this version posted February 17, 2021. The copyright holder for this preprint (which was not certified by peer review) is the author/funder, who has granted bioRxiv a license to display the preprint in perpetuity. It is made available under aCC-BY 4.0 International license.

413 **Materials and Methods**

414 **Mice and Study Approval**

415 *Col6a1*^{Cre} mice were described before [30]. *Rosa26*$^{mT/mG}$ and *Rosa26*^{iDTR} mice were
416 purchased from the Jackson Laboratory [22, 27]. All mice were maintained under
417 specific pathogen free conditions in the Animal House of the Biomedical Sciences
418 Research Center "Alexander Fleming". All studies were approved by the Institutional
419 Committee of Protocol Evaluation in conjunction with the Veterinary Service
420 Management of the Hellenic Republic Prefecture of Attika according to all current
421 European and national legislation and performed in accordance with the guidance of
422 the Institutional Animal Care and Use Committee of BSRC "Alexander Fleming".

423

424 **DSS colitis induction**

425 DSS-induced colitis was performed as previously described [38]. Briefly, 6-10 month
426 old mice received 2.5% DSS in their drinking water, followed by 1-14 days of regular
427 water. Colitis induction was monitored by measuring weight loss.

428

429 **Diptheria Toxin experiments**

430 *Col6a1*^{DTR}, control iDTR and *Col6a1*^{Cre} mice were subjected to intrarectal
431 administration of 100μl diphtheria toxin (Sigma-Aldrich) dissolved in 0.9% sodium
432 chloride at 20 ng/g body weight. Pregnant mice were injected i.p. for two days (E14.5
433 and E15.5) with 5μg DT.

434

435 **Embryo manipulation**

bioRxiv preprint doi: https://doi.org/10.1101/2021.02.16.431453; this version posted February 17, 2021. The copyright holder for this preprint (which was not certified by peer review) is the author/funder, who has granted bioRxiv a license to display the preprint in perpetuity. It is made available under aCC-BY 4.0 International license.

436 Timed pregnancies were set up by checking vaginal plugs to obtain E13.5, E14.5,
437 E16.5 and E18.5 embryos. Pregnant females were sacrificed by cervical dislocation
438 on the specific post coitum day and embryos were dissected in ice-cold PBS. Embryos
439 were fixed overnight in 4% PFA/PBS, immersed in serial solutions of 15% and 30%
440 sucrose/PBS and embedded in OCT for cryosection preparations.

441

442 **Isolation and culture of IMCs**

443 Isolation and culture of IMCs was performed as previously described [39]. Briefly,
444 the colon or small intestine was removed and digested as described above. The cell
445 pellet was resuspended in culture medium, consisting of DMEM (Biochrom), 10%
446 FBS (Biochrom), 100 U/mL penicillin/100 mg/mL streptomycin (Gibco), 2 mM L-
447 Glutamine (Gibco), 1 µg/ml amphotericin B (Sigma) and 1% non-essential amino
448 acids (Gibco) and plated in cell culture flasks. The medium was changed after 3-24
449 hours and cells were used after 2-4 days.

450

451 **Lightsheet Microscopy**

452 For Lightsheet microscopy, the intestine of the embryos was isolated and fixed in 4%
453 PFA/PBS overnight. Tissue clearing was achieved using the Scale A2 clearing
454 solution for 2 weeks [41]. The Lightsheet Z.1 from ZEISS, equipped with sample
455 chamber and Clr Plan-Apochromat 20x/1.0, Corr nd=1.38 lens was used for
456 experiments with tissue cleared by Scale medium, which has a refractive index of
457 n=1.38. Quantification of villi was performed using the Imaris Software.

458

459 **Immunohistochemistry**

bioRxiv preprint doi: https://doi.org/10.1101/2021.02.16.431453; this version posted February 17, 2021. The copyright holder for this preprint (which was not certified by peer review) is the author/funder, who has granted bioRxiv a license to display the preprint in perpetuity. It is made available under aCC-BY 4.0 International license.

460 For confocal microscopy and immunohistochemistry, mice were perfused with 4%
461 PFA prior to the resection of the colon or small intestine. The tissue was then
462 incubated in 4% PFA/PBS overnight and either immersed in serial solutions of 15%
463 and 30% sucrose/PBS and embedded in OCT (VWR Chemicals) for cryosection
464 preparations or in 2% agarose for sectioning with a vibratome (Leica). Sections were
465 subsequently blocked using 1%BSA in TBS containing 0.05% Tween 20 (Sigma)
466 (TTBS) and stained with antibodies listed in Table 1. Staining for CD201 was
467 performed in unfixed tissue, embedded in 4% agarose in CO_2 independent medium
468 (ThermoFisher) and sectioned with vibratome. Sections were blocked in 5% FBS in
469 CO2 independent medium and stained with anti-CD201 antibody. 2hr fixation in 4%
470 PFA/PBS followed prior to the addition of secondary antibody. Mounting medium
471 containing DAPI (Sigma-Aldrich) was used to stain the nuclei. Images were acquired
472 with a Leica TCS SP8X White Light Laser confocal system.

473 For histopathology, colon tissues were fixed in 10% formalin and embedded in
474 paraffin. FFPE sections were stained with hematoxylin (Sigma-Aldrich) and eosin
475 (Sigma-Aldrich) and colitis score assessment was performed as previously described
476 [40]. Stainings for epithelial cell differentiation markers were performed in FFPE
477 section using the antibodies listed in Supplemental Table S1. Signal detection and
478 development were performed using Vectastain ABC-HRP Kit and ImmPACT DAB
479 kit (Vector laboratories). Quantification of proliferating cells was performed in mice
480 that were injected i.p. with 100 mg/kg BrdU (Sigma-Aldrich) 2h prior to sacrificing
481 them, using the BrdU detection kit (BD), according to the manufacturer's instructions.
482 The number of $BrdU^+$ cells was quantified in at least 30 intact, well-oriented crypts
483 per mouse.

484

bioRxiv preprint doi: https://doi.org/10.1101/2021.02.16.431453; this version posted February 17, 2021. The copyright holder for this preprint (which was not certified by peer review) is the author/funder, who has granted bioRxiv a license to display the preprint in perpetuity. It is made available under aCC-BY 4.0 International license.

485 **FACS analysis and sorting**

486 Intestinal tissue preparations were prepared as previously described [21]. Briefly,
487 colon or small intestine was removed, flushed with HBSS (Gibco), containing
488 antibiotic-antimycotic solution (Gibco) and cut into pieces. Intestinal pieces were
489 incubated with HBSS, containing 5mM EDTA, DTT and Penicillin/Streptomycin
490 (Gibco) for 30 min, at 37°C, to remove epithelial cells. After vigorous shaking, the
491 remaining pieces were digested using 300 U/ml Collagenase XI (Sigma-Aldrich), 1
492 mg/ml Dispase II (Roche) and 100 U/ml Dnase I (Sigma-Aldrich) for 40-60 minutes
493 at 37°C. For embryos, the intestine of the embryos was isolated, cut into pieces and
494 digested using 100 μg/ml Collagenase P (Roche), 800 μg/ml Dispase II (Roche), 200
495 μg/ml Dnase I (Sigma-Aldrich) for 20 min at 37°C. The cell suspension was passed
496 through a 70μm strainer, centrifuged and resuspended in FACS buffer (PBS with 2%
497 FBS). For stainings, 1-2 million cells/ 100μl were incubated with the antibodies
498 shown in Supplemental Table S1. For intracellular stainings, cells were fixed and
499 permeabilized using the Fixation and Permeabilization Buffer Set (eBioscience),
500 according to manufacturer's instructions. Propidium Iodide (Sigma) or the Zombie-
501 NIR Fixable Viability Kit (Biolegend) was used for live-dead cell discrimination.
502 Samples were analyzed using the FACSCanto II flow cytometer (BD) or the
503 FACSAria III cell sorter (BD) and the FACSDiva (BD) or FlowJo software (FlowJo,
504 LLC).

505

506 **Table 1. Antibodies used in flow cytometry and immunohistochemistry.**

Antibody against	Conjugate	Clone/Cat. Number	Company	Use
CD45	APC/Cy7	30-F11	BioLegend	FC
CD45	A700	30-F11	BioLegend	FC
CD326 (EpCAM)	APC-efluor780	G8.8	eBioscience	FC

bioRxiv preprint doi: https://doi.org/10.1101/2021.02.16.431453; this version posted February 17, 2021. The copyright holder for this preprint (which was not certified by peer review) is the author/funder, who has granted bioRxiv a license to display the preprint in perpetuity. It is made available under aCC-BY 4.0 International license.

CD326 (EpCAM)	Unconjugated	G8.8	eBioscience	IHC
Ter119	Biotin	TER-119	eBioscience	FC
Ter119	APC-efluor780	TER-119	eBioscience	FC
CD31	Biotin	MEC13.3	BD Pharmingen	FC
CD31	APC/Fire 750	390	BioLegend	FC
Podoplanin	PE/Cy7	8.1.1	BioLegend	FC
Podoplanin	Unconjugated	14-5381-81	eBioscience	IHC
PDGFRα (CD140α)	Unconjugated	#AF1062	R&D Systems	IHC
PDGFRα (CD140α)	APC	APA5	eBioscience	FC
α-SMA	FITC	1A4	Sigma	FC, IHC
α-SMA	efluor660	1A4	Invitrogen	FC, IHC
α-SMA	Cy3	1A4	Sigma	IHC
CD201	APC	eBio1560	eBioscience	FC, IHC
CD201	PE/Cy5	eBio1560	Invitrogen	FC, IHC
CD34	Biotin	RAM34	eBioscience	FC, IHC
Streptavidin	A750	S21384	Invitrogen	FC
Streptavidin	A647	S32357	Invitrogen	FC
Streptavidin	PE	554061	BD Pharmingen	FC
Streptavidin	Brilliant Violet 421	405225	BioLegend	FC
Rabbit IgG	A647	A21244	Invitrogen	IHC
Rat IgG	A594	A11007	Invitrogen	IHC
Rat IgG	A647	A21247	Invitrogen	IHC
Goat IgG	A647	A11056	Invitrogen	IHC
Hamster IgG	A647	A21451	Invitrogen	IHC
Dclk1	Unconjugated	Ab109029	Abcam	IHC
ChgA	Unconjugated	Ab15160	Abcam	IHC
Ki67	Unconjugated	Ab15580	Abcam	IHC
BrdU	APC	552598	BD Pharmingen	FC

*FC, Flow Cytometry; IHC, Immunohistochemistry

Crypt isolation and co-culture with IMCs

Intestinal crypts were isolated as described previously [42]. Briefly, the small intestine was flashed with cold PBS (Gibco), opened longitudinally and villi were scraped off using a coverslip. Then, it was cut into 5mm pieces and washed extensively until the supernatant was clear. Ice-cold crypt isolation buffer (2 mM EDTA in PBS) was added to the fragments and stirred for 1 hour at 4°C. Fragments were allowed to settle down, the supernatant was removed and ice-cold 2 mM EDTA/PBS was added followed by pipetting up and down. Released crypts were passed through a 70-μm-cell strainer and the procedure was repeated until most of

bioRxiv preprint doi: https://doi.org/10.1101/2021.02.16.431453; this version posted February 17, 2021. The copyright holder for this preprint (which was not certified by peer review) is the author/funder, who has granted bioRxiv a license to display the preprint in perpetuity. It is made available under aCC-BY 4.0 International license.

518 crypts were released. Crypt fractions were centrifuged at 300*g* for 5 minutes and
519 resuspended with ice-cold basal culture medium (Advanced DMEM/F12 (Gibco)
520 supplemented with 2 mM GlutaMax (Gibco), 10 mM HEPES (Gibco) and 100 U/mL
521 penicillin/ 100 mg/mL streptomycin (Gibco). Crypts were centrifuged again at 200*g*
522 for 5 minutes, resuspended in warm basal culture medium and counted. Crypts were
523 mixed with ColVIcre-GFP$^+$ and GFP$^-$ IMCs sorted by FACS at passage 1 and
524 subsequently resuspended in Matrigel (BD Biosciences) at 250 crypts/50.000
525 IMCs/30 μl in 48-well plates. After Matrigel polymerization, culture medium was
526 added in the wells, consisting of DMEM/F12 medium (Gibco), Glutamax (Gibco),
527 Penicillin/Streptomycin, N2 supplement (Life Technologies, 1×), B27 supplement
528 (Life Technologies, 1×), and 1 mM N-acetylcysteine (Sigma-Aldrich), 50 ng/ml EGF
529 (Life Technologies), 100 ng/ml Noggin (PeproTech) and Rspo1 (PeproTech) where
530 indicated. Images were acquired with the Zeiss Axio Observer Z1 microscope.
531 Organoid measurements were performed using the ImageJ/Fiji software.

532

533 **RNA isolation and qRT-PCR**

534 RNA was isolated using the RNeasy mini kit or the RNeasy micro kit (Qiagen),
535 depending on the number of cells, according to the manufacturer's instruction. 100ng-
536 1μg of RNA was used to generate cDNA using the MMLV reverse transcriptase by
537 Promega and oligo-dT primers (Promega), according to the manufacturer's
538 instructions. For qRT-PCR, the SYBR Green PCR Master Mix (Invitrogen) was used
539 according to the manufacturer's instructions. Forward and reverse primers were added
540 at a concentration of 0.2 pmol/ml in a final volume of 20 μl and qRT-PCR was
541 performed on a CFX96 Touch™ Real-Time PCR Detection System (Bio-Rad). The
542 primer list can be found in Table 2.

bioRxiv preprint doi: https://doi.org/10.1101/2021.02.16.431453; this version posted February 17, 2021. The copyright holder for this preprint (which was not certified by peer review) is the author/funder, who has granted bioRxiv a license to display the preprint in perpetuity. It is made available under aCC-BY 4.0 International license.

543

544

545 **Table 2. List of primers used for real-time PCR.**

Gene	Sequence (5'— 3')	Product (bp)
Bmp2	F: ACCCCCAGCAAGGACGTCGT R: TGGAAGCTGCGCACGGTGTT	137
Bmp3	F: TTTGCTGATATCGGCTGGAG R: TGGTGGCGTGATTTGATG	125
Bmp4	F: CCCGCAGAAGGGCCAAAC R: TAGCCGGGTGGGGCCACAAT	138
Bmp5	F: ACCTCTTGCCAGCCTACATG R: TGCTGCTGTCACTGCTTCTC	169
Bmp7	F: TCCAAGACGCCAAAGAACCA R: TGCAATGATCCAGTCCTGCC	140
Wnt5a	F: GGTGCCATGTCTTCCAAGTT R: TGAGAAAGTCCTGCCAGTTG	176
Ednrb	F: TTGCGAGAGGCCTGTTTAGG R: GAGACCAACTCGTGCGGATT	136
Cspg4	F: GGATGCCTCCAGGTCAGACT R: CTCCGTCAACAGACAGCACA	142
Casq2	F: GCCCAACGTCATCCCTAACA R: CCCATTCAAGTCGTCTTCCCAT	133
Kcnj8	F: CAAACCCGAGTCTGAGGACG R: TTCCTTTCACCATAGCCCGC	81
Foxl1	F: ATAAACCAGGCTCCCCTTTG R: AGCCAAAGTACGTGCCAAAC	75
ChgA	F: CCAAGGTGATGAAGTGCGTC R: GGTGTCGCAGGATAGAGAGGA	129
Lgr5	F: CCTACTCGAAGACTTACCCAGT R: GCATTGGGGTGAATGATAGCA	165
Ascl2	F: AAGCACACCTTGACTGGTACG R: AAGTGGACGTTTGCACCTTCA	115
Hprt	F: TGCCGAGGATTTGGAAAAAGTG R: CACAGAGGGCCACAATGTGATG	116
Cox6c	F: CTGAGCCAAGAAAGAAGGCG R: TGAACTTCTTTGGAGCGCAA	149
B2m	F: TTCTGGTGCTTGTCTCACTGA R: CAGTATGTTCGGCTTCCCATTC	103

546

547

548 **3' RNAseq sequencing and analysis**

549 The quantity and quality of RNA samples from sorted cells were analyzed using the
550 bioanalyzer form Agilent in combination with the Agilent RNA 6000 Nano. RNA

bioRxiv preprint doi: https://doi.org/10.1101/2021.02.16.431453; this version posted February 17, 2021. The copyright holder for this preprint (which was not certified by peer review) is the author/funder, who has granted bioRxiv a license to display the preprint in perpetuity. It is made available under aCC-BY 4.0 International license.

551 samples with RNA Integrity Number (RIN) > 7 were further used for library
552 preparation using the 3' mRNA-Seq Library Prep Kit Protocol for Ion Torrent
553 (QuantSeq-LEXOGEN™) according to manufacturer's instructions. The quantity and
554 quality of libraries were assessed using the DNA High Sensitivity Kit in the
555 bioanalyzer, according to the manufacturer's instructions (Agilent). Libraries were
556 subsequently pooled and templated using the Ion PI IC200 Chef Kit (ThermoFisher
557 Scientific) on an Ion Proton Chef Instrument or Ion One Touch System. Sequencing
558 was performed using the Ion PI™ Sequencing 200 V3 Kit and Ion Proton PI™ V2
559 chips (ThermoFisher Scientific) on an Ion Proton™ System, according to the
560 manufacturer's instructions. The RNA-Seq FASTQ files were mapped using
561 TopHat2 [43], with default settings and using additional transcript annotation data
562 for the mm10 genome from Illumina iGenomes
563 (https://support.illumina.com/sequencing/sequencing_software/igenome.html).
564 According to the Ion Proton manufacturers recommendation, the reads which
565 remained unmapped were submitted to a second round of mapping using Bowtie2
566 [44] against the mm10 genome with the very-sensitive switch turned on and
567 merged with the initial mappings. Through metaseqr R package [45],
568 GenomicRanges and DESeq were employed in order to summarize bam files of the
569 previous step to read counts table and to perform differential expression analysis
570 (after removing genes that had zero counts over all the RNA-Seq samples).

571 Downstream bioinformatics analysis and visualization tasks were performed using
572 InteractiveVenn for Venn diagrams (www.interactivenn.net) [46] and the Functional
573 Annotation tool from DAVID for Gene Ontologies (david.ncifcrf.gov) [47, 48].
574 Volcano plots and heatmaps were generated in R using an in-house developed script
575 utilizing the packages ggplot2, gplots and pheatmap (https://cran.r-

bioRxiv preprint doi: https://doi.org/10.1101/2021.02.16.431453; this version posted February 17, 2021. The copyright holder for this preprint (which was not certified by peer review) is the author/funder, who has granted bioRxiv a license to display the preprint in perpetuity. It is made available under aCC-BY 4.0 International license.

576 project.org/web/packages/pheatmap/index.html) [49-51]. RNA-seq datasets have been
577 deposited in NCBI's Gene Expression Omnibus [52] and are accessible through the
578 GEO Series accession number GSE117308.
579

580 **Comparison with single cell datasets**

581 The positive cluster marker genes of the healthy and DSS treated mouse, from the
582 public dataset GSE114374, were used as gene signatures for each cell type identified
583 in the single cell analysis. For each gene of a signature z-scores of log2 normalized
584 expression values were calculated for the bulk RNA-seq samples GC(GC1, GC2,
585 GC3), TC(TC1, TC2, TC3), UC(UC1, UC2, UC3) and GDS(GDS1, GDS2, GDS3),
586 TDS(TDS1, TDS2, TDS3), UDS(UDS1, UDS2, UDS3). In the boxplots of Figure 1G
587 and 5D the mean z-score of GC1, GC2, GC3 and GDS1, GDS2, GDS3 are displayed
588 respectively.
589

590 **Statistical analysis**

591 Data are presented as mean ± SD. Statistical significance was calculated by Student's
592 t-test or one-way ANOVA for multiple comparisons. The D'Agostino Pearson test
593 was used to test if the dataset followed a normal distribution. Welch's correction was
594 used for samples that showed unequal variance. P-values ≤ 0.05 were considered
595 significant. Data were analysed using the GraphPad Prism 8 software.
596

597 **Acknowledgements**

598 We would like to thank Michalis Meletiou for mouse genotyping. We would also like
599 to thank the Genomics Facility of BSRC "Alexander Fleming", and specifically

bioRxiv preprint doi: https://doi.org/10.1101/2021.02.16.431453; this version posted February 17, 2021. The copyright holder for this preprint (which was not certified by peer review) is the author/funder, who has granted bioRxiv a license to display the preprint in perpetuity. It is made available under aCC-BY 4.0 International license.

600 Vaggelis Harokopos for performing all RNA sequencing experiments and Martin
601 Reczko and Panagiotis Moulos for initial bioinformatics analyses. We acknowledge
602 support of this work by the InfrafrontierGR Infrastructure, co-funded by Greece and
603 the European Union (European Regional Development Fund), under NSRF 2014-
604 2020, MIS 5002135), which provided mouse hosting and phenotyping facilities,
605 including, histopathology, flow cytometry, and advanced microscopy facilities. This
606 work was supported by a grant from the Stavros Niarchos Foundation to the BSRC
607 "Alexander Fleming" as part of the Foundation's initiative to support the Greek
608 research center ecosystem, a grant from the Hellenic Foundation for Research &
609 Innovation (H.F.R.I.) to MES (Grant No 1687), the FP7 Advanced ERC grant MCs-
610 inTEST (Grant Agreement No 340217) to GK, a grant from the European Crohn's
611 and Colitis Organisation to VK and a grant from the Fondation Sante to VK.
612
613

bioRxiv preprint doi: https://doi.org/10.1101/2021.02.16.431453; this version posted February 17, 2021. The copyright holder for this preprint (which was not certified by peer review) is the author/funder, who has granted bioRxiv a license to display the preprint in perpetuity. It is made available under aCC-BY 4.0 International license.

614 **References**

615 [1] Gehart H, Clevers H. Tales from the crypt: new insights into intestinal stem
616 cells. Nat Rev Gastroenterol Hepatol 2019;16(1):19-34.
617 [2] de Sousa E Melo F, de Sauvage FJ. Cellular Plasticity in Intestinal
618 Homeostasis and Disease. Cell Stem Cell 2019;24(1):54-64.
619 [3] Powell DW, Pinchuk IV, Saada JI, Chen X, Mifflin RC. Mesenchymal cells of
620 the intestinal lamina propria. Annu Rev Physiol 2011;73:213-37.
621 [4] McCarthy N, Kraiczy J, Shivdasani RA. Cellular and molecular architecture of
622 the intestinal stem cell niche. Nat Cell Biol 2020;22(9):1033-41.
623 [5] Kabiri Z, Greicius G, Madan B, Biechele S, Zhong Z, Zaribafzadeh H, Edison,
624 Aliyev J, Wu Y, Bunte R, Williams BO, Rossant J, Virshup DM. Stroma
625 provides an intestinal stem cell niche in the absence of epithelial Wnts.
626 Development 2014;141(11):2206-15.
627 [6] Aoki R, Shoshkes-Carmel M, Gao N, Shin S, May CL, Golson ML, Zahm
628 AM, Ray M, Wiser CL, Wright CV, Kaestner KH. Foxl1-expressing
629 mesenchymal cells constitute the intestinal stem cell niche. Cell Mol
630 Gastroenterol Hepatol 2016;2(2):175-88.
631 [7] McCarthy N, Manieri E, Storm EE, Saadatpour A, Luoma AM, Kapoor VN,
632 Madha S, Gaynor LT, Cox C, Keerthivasan S, Wucherpfennig K, Yuan GC,
633 de Sauvage FJ, Turley SJ, Shivdasani RA. Distinct Mesenchymal Cell
634 Populations Generate the Essential Intestinal BMP Signaling Gradient. Cell
635 Stem Cell 2020;26(3):391-402.e5.
636 [8] Kosinski C, Li VS, Chan AS, Zhang J, Ho C, Tsui WY, Chan TL, Mifflin RC,
637 Powell DW, Yuen ST, Leung SY, Chen X. Gene expression patterns of human

bioRxiv preprint doi: https://doi.org/10.1101/2021.02.16.431453; this version posted February 17, 2021. The copyright holder for this preprint (which was not certified by peer review) is the author/funder, who has granted bioRxiv a license to display the preprint in perpetuity. It is made available under aCC-BY 4.0 International license.

638 colon tops and basal crypts and BMP antagonists as intestinal stem cell niche
639 factors. Proc Natl Acad Sci U S A 2007;104(39):15418-23.
640 [9] Beumer J, Artegiani B, Post Y, Reimann F, Gribble F, Nguyen TN, Zeng H,
641 Van den Born M, Van Es JH, Clevers H. Enteroendocrine cells switch
642 hormone expression along the crypt-to-villus BMP signalling gradient. Nat
643 Cell Biol 2018;20(8):909-16.
644 [10] Walton KD, Freddo AM, Wang S, Gumucio DL. Generation of intestinal
645 surface: an absorbing tale. Development 2016;143(13):2261-72.
646 [11] Koliaraki V, Prados A, Armaka M, Kollias G. The mesenchymal context in
647 inflammation, immunity and cancer. Nat Immunol 2020;21(9):974-82.
648 [12] Greicius G, Kabiri Z, Sigmundsson K, Liang C, Bunte R, Singh MK, Virshup
649 DM. PDGFRalpha(+) pericryptal stromal cells are the critical source of Wnts
650 and RSPO3 for murine intestinal stem cells in vivo. Proc Natl Acad Sci U S A
651 2018;115(14):E3173-E81.
652 [13] Shoshkes-Carmel M, Wang YJ, Wangensteen KJ, Tóth B, Kondo A, Massasa
653 EE, Itzkovitz S, Kaestner KH. Subepithelial telocytes are an important source
654 of Wnts that supports intestinal crypts. Nature 2018;557(7704):242-6.
655 [14] Kinchen J, Chen HH, Parikh K, Antanaviciute A, Jagielowicz M, Fawkner-
656 Corbett D, Ashley N, Cubitt L, Mellado-Gomez E, Attar M, Sharma E, Wills
657 Q, Bowden R, Richter FC, Ahern D, Puri KD, Henault J, Gervais F, Koohy H,
658 Simmons A. Structural Remodeling of the Human Colonic Mesenchyme in
659 Inflammatory Bowel Disease. Cell 2018;175(2):372-86.e17.
660 [15] Smillie CS, Biton M, Ordovas-Montanes J, Sullivan KM, Burgin G, Graham
661 DB, Herbst RH, Rogel N, Slyper M, Waldman J, Sud M, Andrews E, Velonias
662 G, Haber AL, Jagadeesh K, Vickovic S, Yao J, Stevens C, Dionne D, Nguyen

bioRxiv preprint doi: https://doi.org/10.1101/2021.02.16.431453; this version posted February 17, 2021. The copyright holder for this preprint (which was not certified by peer review) is the author/funder, who has granted bioRxiv a license to display the preprint in perpetuity. It is made available under aCC-BY 4.0 International license.

663 LT, Villani AC, Hofree M, Creasey EA, Huang H, Rozenblatt-Rosen O,
664 Garber JJ, Khalili H, Desch AN, Daly MJ, Ananthakrishnan AN, Shalek AK,
665 Xavier RJ, Regev A. Intra- and Inter-cellular Rewiring of the Human Colon
666 during Ulcerative Colitis. Cell 2019;178(3):714-30.e22.
667 [16] Kim JE, Fei L, Yin WC, Coquenlorge S, Rao-Bhatia A, Zhang X, Shi SSW,
668 Lee JH, Hahn NA, Rizvi W, Kim KH, Sung HK, Hui CC, Guo G, Kim TH.
669 Single cell and genetic analyses reveal conserved populations and signaling
670 mechanisms of gastrointestinal stromal niches. Nat Commun 2020;11(1):334.
671 [17] Stzepourginski I, Nigro G, Jacob JM, Dulauroy S, Sansonetti PJ, Eberl G,
672 Peduto L. CD34+ mesenchymal cells are a major component of the intestinal
673 stem cells niche at homeostasis and after injury. Proc Natl Acad Sci U S A
674 2017;114(4):E506-E13.
675 [18] Degirmenci B, Valenta T, Dimitrieva S, Hausmann G, Basler K. GLI1-
676 expressing mesenchymal cells form the essential Wnt-secreting niche for
677 colon stem cells. Nature 2018;558(7710):449-53.
678 [19] Bahar Halpern K, Massalha H, Zwick RK, Moor AE, Castillo-Azofeifa D,
679 Rozenberg M, Farack L, Egozi A, Miller DR, Averbukh I, Harnik Y,
680 Weinberg-Corem N, de Sauvage FJ, Amit I, Klein OD, Shoshkes-Carmel M,
681 Itzkovitz S. Lgr5+ telocytes are a signaling source at the intestinal villus tip.
682 Nat Commun 2020;11(1):1936.
683 [20] Martin JC, Chang C, Boschetti G, Ungaro R, Giri M, Grout JA, Gettler K,
684 Chuang LS, Nayar S, Greenstein AJ, Dubinsky M, Walker L, Leader A, Fine
685 JS, Whitehurst CE, Mbow ML, Kugathasan S, Denson LA, Hyams JS,
686 Friedman JR, Desai PT, Ko HM, Laface I, Akturk G, Schadt EE, Salmon H,
687 Gnjatic S, Rahman AH, Merad M, Cho JH, Kenigsberg E. Single-Cell

bioRxiv preprint doi: https://doi.org/10.1101/2021.02.16.431453; this version posted February 17, 2021. The copyright holder for this preprint (which was not certified by peer review) is the author/funder, who has granted bioRxiv a license to display the preprint in perpetuity. It is made available under aCC-BY 4.0 International license.

688 Analysis of Crohn's Disease Lesions Identifies a Pathogenic Cellular Module
689 Associated with Resistance to Anti-TNF Therapy. Cell 2019;178(6):1493-
690 508.e20.
691 [21] Koliaraki V, Pasparakis M, Kollias G. IKKbeta in intestinal mesenchymal
692 cells promotes initiation of colitis-associated cancer. J Exp Med
693 2015;212(13):2235-51.
694 [22] Muzumdar MD, Tasic B, Miyamichi K, Li L, Luo L. A global double-
695 fluorescent Cre reporter mouse. Genesis 2007;45(9):593-605.
696 [23] Prados A, Kollias G, Koliaraki V. CollagenVI-Cre mice: A new tool to target
697 stromal cells in secondary lymphoid organs. Sci Rep 2016;6:33027.
698 [24] Walton KD, Kolterud A, Czerwinski MJ, Bell MJ, Prakash A, Kushwaha J,
699 Grosse AS, Schnell S, Gumucio DL. Hedgehog-responsive mesenchymal
700 clusters direct patterning and emergence of intestinal villi. Proc Natl Acad Sci
701 U S A 2012;109(39):15817-22.
702 [25] Walton KD, Whidden M, Kolterud A, Shoffner SK, Czerwinski MJ,
703 Kushwaha J, Parmar N, Chandhrasekhar D, Freddo AM, Schnell S, Gumucio
704 DL. Villification in the mouse: Bmp signals control intestinal villus patterning.
705 Development 2016;143(3):427-36.
706 [26] Karlsson L, Lindahl P, Heath JK, Betsholtz C. Abnormal gastrointestinal
707 development in PDGF-A and PDGFR-(alpha) deficient mice implicates a
708 novel mesenchymal structure with putative instructive properties in villus
709 morphogenesis. Development 2000;127(16):3457-66.
710 [27] Buch T, Heppner FL, Tertilt C, Heinen TJ, Kremer M, Wunderlich FT, Jung
711 S, Waisman A. A Cre-inducible diphtheria toxin receptor mediates cell lineage
712 ablation after toxin administration. Nat Methods 2005;2(6):419-26.

bioRxiv preprint doi: https://doi.org/10.1101/2021.02.16.431453; this version posted February 17, 2021. The copyright holder for this preprint (which was not certified by peer review) is the author/funder, who has granted bioRxiv a license to display the preprint in perpetuity. It is made available under aCC-BY 4.0 International license.

713 [28] Qi Z, Li Y, Zhao B, Xu C, Liu Y, Li H, Zhang B, Wang X, Yang X, Xie W, Li
714 B, Han J-DJ, Chen Y-G. BMP restricts stemness of intestinal Lgr5 + stem
715 cells by directly suppressing their signature genes. Nature Communications
716 2017;8(1):1-14.
717 [29] Brügger MD, Valenta T, Fazilaty H, Hausmann G, Basler K. Distinct
718 populations of crypt-associated fibroblasts act as signaling hubs to control
719 colon homeostasis. PLoS Biol 2020;18(12):e3001032.
720 [30] Armaka M, Apostolaki M, Jacques P, Kontoyiannis DL, Elewaut D, Kollias
721 G. Mesenchymal cell targeting by TNF as a common pathogenic principle in
722 chronic inflammatory joint and intestinal diseases. J Exp Med
723 2008;205(2):331-7.
724 [31] Shyer AE, Tallinen T, Nerurkar NL, Wei Z, Gil ES, Kaplan DL, Tabin CJ,
725 Mahadevan L. Villification: how the gut gets its villi. Science
726 2013;342(6155):212-8.
727 [32] Shyer AE, Huycke TR, Lee C, Mahadevan L, Tabin CJ. Bending gradients:
728 how the intestinal stem cell gets its home. Cell 2015;161(3):569-80.
729 [33] Roulis M, Kaklamanos A, Schernthanner M, Bielecki P, Zhao J, Kaffe E,
730 Frommelt L-S, Qu R, Knapp MS, Henriques A, Chalkidi N, Koliaraki V, Jiao
731 J, Brewer R, Bacher M, Blackburn HN, Zhao X, Breyer RM, Aidinis V, Jain
732 D, Su B, Herschman HR, Kluger Y, Kollias G, Flavell RA. Paracrine
733 orchestration of intestinal tumorigenesis by a confined mesenchymal niche.
734 Nature 2020.
735 [34] Kaestner KH, Silberg DG, Traber PG, Schütz G. The mesenchymal winged
736 helix transcription factor Fkh6 is required for the control of gastrointestinal
737 proliferation and differentiation. Genes Dev 1997;11(12):1583-95.

bioRxiv preprint doi: https://doi.org/10.1101/2021.02.16.431453; this version posted February 17, 2021. The copyright holder for this preprint (which was not certified by peer review) is the author/funder, who has granted bioRxiv a license to display the preprint in perpetuity. It is made available under aCC-BY 4.0 International license.

738 [35] Holloway EM, Czerwinski M, Tsai YH, Wu JH, Wu A, Childs CJ, Walton
739 KD, Sweet CW, Yu Q, Glass I, Treutlein B, Camp JG, Spence JR. Mapping
740 Development of the Human Intestinal Niche at Single-Cell Resolution. Cell
741 Stem Cell 2020.
742 [36] Kim HS, Neugebauer J, McKnite A, Tilak A, Christian JL. BMP7 functions
743 predominantly as a heterodimer with BMP2 or BMP4 during mammalian
744 embryogenesis. Elife 2019;8.
745 [37] Worthley DL, Churchill M, Compton JT, Tailor Y, Rao M, Si Y, Levin D,
746 Schwartz MG, Uygur A, Hayakawa Y, Gross S, Renz BW, Setlik W, Martinez
747 AN, Chen X, Nizami S, Lee HG, Kang HP, Caldwell JM, Asfaha S,
748 Westphalen CB, Graham T, Jin G, Nagar K, Wang H, Kheirbek MA, Kolhe A,
749 Carpenter J, Glaire M, Nair A, Renders S, Manieri N, Muthupalani S, Fox JG,
750 Reichert M, Giraud AS, Schwabe RF, Pradere JP, Walton K, Prakash A,
751 Gumucio D, Rustgi AK, Stappenbeck TS, Friedman RA, Gershon MD, Sims
752 P, Grikscheit T, Lee FY, Karsenty G, Mukherjee S, Wang TC. Gremlin 1
753 identifies a skeletal stem cell with bone, cartilage, and reticular stromal
754 potential. Cell 2015;160(1-2):269-84.
755 [38] Wirtz S, Popp V, Kindermann M, Gerlach K, Weigmann B, Fichtner-Feigl S,
756 Neurath MF. Chemically induced mouse models of acute and chronic
757 intestinal inflammation. Nat Protoc 2017;12(7):1295-309.
758 [39] Koliaraki V, Kollias G. Isolation of intestinal mesenchymal cells from adult
759 mice. Bio-protocol 2016;6(18):e1940.
760 [40] Koliaraki V, Roulis M, Kollias G. Tpl2 regulates intestinal myofibroblast
761 HGF release to suppress colitis-associated tumorigenesis. J Clin Invest
762 2012;122(11):4231-42.

bioRxiv preprint doi: https://doi.org/10.1101/2021.02.16.431453; this version posted February 17, 2021. The copyright holder for this preprint (which was not certified by peer review) is the author/funder, who has granted bioRxiv a license to display the preprint in perpetuity. It is made available under aCC-BY 4.0 International license.

763 [41] Hama H, Kurokawa H, Kawano H, Ando R, Shimogori T, Noda H, Fukami K,
764 Sakaue-Sawano A, Miyawaki A. Scale: a chemical approach for fluorescence
765 imaging and reconstruction of transparent mouse brain. Nat Neurosci
766 2011;14(11):1481-8.
767 [42] Sato T, Vries RG, Snippert HJ, van de Wetering M, Barker N, Stange DE, van
768 Es JH, Abo A, Kujala P, Peters PJ, Clevers H. Single Lgr5 stem cells build
769 crypt-villus structures in vitro without a mesenchymal niche. Nature
770 2009;459(7244):262-5.
771 [43] Kim D, Pertea G, Trapnell C, Pimentel H, Kelley R, Salzberg SL. TopHat2:
772 accurate alignment of transcriptomes in the presence of insertions, deletions
773 and gene fusions. Genome Biol 2013;14(4):R36.
774 [44] Langmead B, Salzberg SL. Fast gapped-read alignment with Bowtie 2. Nat
775 Methods 2012;9(4):357-9.
776 [45] Moulos P, Hatzis P. Systematic integration of RNA-Seq statistical algorithms
777 for accurate detection of differential gene expression patterns. Nucleic Acids
778 Res 2015;43(4):e25.
779 [46] Heberle H, Meirelles GV, da Silva FR, Telles GP, Minghim R. InteractiVenn:
780 a web-based tool for the analysis of sets through Venn diagrams. BMC
781 Bioinformatics 2015;16:169.
782 [47] Huang da W, Sherman BT, Lempicki RA. Bioinformatics enrichment tools:
783 paths toward the comprehensive functional analysis of large gene lists.
784 Nucleic Acids Res 2009;37(1):1-13.
785 [48] Huang da W, Sherman BT, Lempicki RA. Systematic and integrative analysis
786 of large gene lists using DAVID bioinformatics resources. Nat Protoc
787 2009;4(1):44-57.

bioRxiv preprint doi: https://doi.org/10.1101/2021.02.16.431453; this version posted February 17, 2021. The copyright holder for this preprint (which was not certified by peer review) is the author/funder, who has granted bioRxiv a license to display the preprint in perpetuity. It is made available under aCC-BY 4.0 International license.

788 [49] Wickham H. ggplot2: Elegant Graphics for Data Analysis. New York:
789 Springer Publishing Company, Incorporated. 2016.
790 [50] Warnes GR, Bolker B, Bonebakker L, Gentleman R, Huber W, Liaw A,
791 Lumley T, Maechler M, Magnusson A, Moeller S, Schwartz M, Venables B.
792 gplots: Various R Programming Tools for Plotting Data. 2016.
793 [51] Team RC. R: A language and environment for statistical computing. R
794 Foundation for Statistical Computing. Vienna, Austria. 2017.
795 [52] Edgar R, Domrachev M, Lash AE. Gene Expression Omnibus: NCBI gene
796 expression and hybridization array data repository. Nucleic Acids Res
797 2002;30(1):207-10.
798

bioRxiv preprint doi: https://doi.org/10.1101/2021.02.16.431453; this version posted February 17, 2021. The copyright holder for this preprint (which was not certified by peer review) is the author/funder, who has granted bioRxiv a license to display the preprint in perpetuity. It is made available under aCC-BY 4.0 International license.

799 **Figure Legends**

800 **Figure 1. The *Col6a1^Cre^* mouse targets CD34⁻ IMCs in the mouse colon.** A) FACS
801 sorting strategy for the isolation of *Col6a1*^{Cre}-GFP^{+} (GC) and *Col6a1*^{Cre}-GFP^{-} (TC)
802 mesenchymal cells from the colon. Single cell preparations from the colon (UC) were
803 stained for the Lin^{+} markers CD45, EpCAM, CD31 and Ter119 and Propidium Iodide
804 (PI) for dead cell exclusion. 3 samples from 4-5 mice each were subsequently
805 analyzed. B) Heatmap of differentially expressed genes in GC vs TC and UC samples,
806 corresponding to GO terms related to epithelial proliferation/differentiation and blood
807 vessel regulation. Log2 transformed normalized read counts of genes are shown. Read
808 counts are scaled per column, red denotes high expression and blue low expression
809 values. C) Representative FACS analysis of CD34 expression in Lin- cells in the
810 colon of *Col6a1*^{mTmG} mice (n = 4-5 mice). D) Immunohistochemical analysis for
811 CD34 expression in the colon of *Col6a1*^{mTmG} mice (n = 9-10 mice, Scale bar: 50 μm).
812 E) Total number and size of intestinal structures after 3 days of co-culture with sorted
813 *Col6a1*-GFP^{+} and GFP^{-} IMCs, with and without R-Spondin 1, respectively. Data
814 represents mean ± SEM from one of four experiments performed in quadruplicates.
815 *p<0.05, **p<0.01, ***p<0.001. F) Representative bright-field images of intestinal
816 organoids co-cultured with *Col6a1*-GFP^{+} and GFP^{-} IMCs at day 3, in the absence of
817 R-Spondin 1 (Scale bar: 100 μm). G) Mean expression (z-score) of genes signatures
818 extracted from the different intestinal mesenchymal clusters identified in Kinchen et
819 al., [14] in *Col6a1*-GFP^{+} bulk RNA-seq samples. MF, myofibroblasts; SMC, smooth
820 muscle cells. H) Heatmap of the top 50 differentially expressed genes in the Str2
821 population (Kinchen et al., [14]) and their relative expression in the GC and TC
822 samples.

823

bioRxiv preprint doi: https://doi.org/10.1101/2021.02.16.431453; this version posted February 17, 2021. The copyright holder for this preprint (which was not certified by peer review) is the author/funder, who has granted bioRxiv a license to display the preprint in perpetuity. It is made available under aCC-BY 4.0 International license.

824 **Figure 2. GFP$^+$/CD201$^+$ mesenchymal cells comprise distinct subsets in the**
825 **mouse colon.** A) Immunohistochemistry for CD201 in the colon of *Col6a1^{mTmG}* mice
826 (n = 4 mice, Scale bar: 50 μm). The dotted line delimitates the epithelial surface
827 towards the lumen. B) Representative FACS analysis of CD201 expression in Lin$^-$
828 cells in the colon of *Col6a1^{mTmG}* mice (n = 10 mice). C) Gene expression analysis of
829 selected genes in FACS-sorted GFP$^+$CD201$^+$, GFP$^+$CD201$^-$ and GFP$^-$ colonic
830 mesenchymal cells from *Col6a1^{mTmG}* mice. Expression is measured in relation to the
831 *Hprt* housekeeping gene (n = 3), *p<0.05, **p<0.01, ***p<0.001. D) tSNE plots
832 showing the expression of CD34, CD201, PDGFRα and αSMA in Lin$^-$ colonic
833 mesenchymal cells using FACS analysis (n = 8 mice). E) Immunohistochemistry for
834 αSMA and CD31 in the colon of *Col6a1^{mTmG}* mice, showing their localization around
835 blood vessels (white arrow) (Scale bar: 50 μm). The bottom of crypts is shown. F)
836 Immunohistochemistry for PDGFRα and CD34 in the colon of *Col6a1^{mTmG}* mice.
837 Different planes are shown. White arrows indicate PDGFRα^{hi} (upper panel) and
838 PDGFRα^{lo} (lower panel) mesenchymal cells (Scale bar: 50 μm). The dotted line
839 delimitates the epithelial surface towards the lumen. G) Confocal imaging of GFP$^+$
840 cells at the top of *Col6a1^{mTmG}* colonic crypts (Scale bar: 10 μm). H)
841 Immunohistochemical analysis of PDGFRα$^+$αSMA^{lo} cells in the colon. White arrows
842 indicate PDGFRα^{lo} mesenchymal cells. (Scale bar = 10 μm) (n = 4 mice for all
843 analyses). I) Quantification of *Col6a1^{Cre}*-GFP$^+$ cells in each mesenchymal subset.
844 Only major categories of CD201$^-$ cells are included (n = 6 mice). K)
845 Immunohistochemistry for CD31 in the colon of *Col6a1^{mTmG}* mice (n = 3 mice, Scale
846 bar: 10 μm).
847

bioRxiv preprint doi: https://doi.org/10.1101/2021.02.16.431453; this version posted February 17, 2021. The copyright holder for this preprint (which was not certified by peer review) is the author/funder, who has granted bioRxiv a license to display the preprint in perpetuity. It is made available under aCC-BY 4.0 International license.

848 **Figure 3. Intestinal telocytes/SEMFs originate from embryonic mesenchymal cell**
849 **aggregates and are necessary for intestinal morphogenesis.** Confocal images
850 showing GFP and PDGFRα expression in A) the small intestine and colon at E15.5
851 (Scale bar = 50 μm) and B) the small intestine and colon of *Col6a1*^{mTmG} mice at the
852 indicated developmental stages (Scale bar = 50 μm), (n = 3 mice per developmental
853 stage). C) Confocal images showing GFP and αSMA expression in the small intestine
854 and colon of *Col6a1*^{mTmG} mice at the indicated developmental stages (Scale bar = 50
855 μm), (n = 3 mice per developmental stage). D) FACS analysis of *Col6a1*-GFP^{+}
856 intestinal mesenchymal cells at E18.5. E) FACS-based quantification of GFP^{+} cells in
857 PDGFRα^{hi} and PDGFRα^{lo} cells in E16.5 and E18.5. F) FACS analysis of GFP^{+} cells
858 in E18.5, showing that they all are CD201^{+}PDGFRα^{hi} cells (n = 3-4 mice per
859 developmental stage in all FACS analyses). G) Schematic representation of DT
860 administration. Pregnant females received two injections of diptheria toxin (DT)
861 (*5*μg) at E14.5 and E15.5, which was followed by ex vivo culture of the intestine from
862 E16.5 to E18.5. H) Lightsheet imaging (maximum projection, Scale bar = 100 μm)
863 and confocal images showing GFP, PDGFRα and αSMA expression (Scale bar = 50
864 μm) in the small intestine of *Col6a1*^{DTR} and control mice. I) quantification of villi/nm
865 in the presence of DT (n = 7). All (GFP^{+} and GFP^{-}) and only GFP^{-} villi are presented
866 in DT treated mice. ***p<0.001, **p<0.01.
867

868 **Figure 4. *Col6a1*$^{Cre+}$ cell depletion leads to deregulated epithelial cell**
869 **differentiation and proliferation during homeostasis.** A) Schematic representation
870 of DT administration in homeostasis. *Col6a1*^{DTR} and control (*Col6a1*^{mTmG}, *iDTR*$^{f/f/}$)
871 mice received 3 daily intrarectal administrations of DT (*20ng/g* body weight) and
872 mice were sacrificed after 5 days. B) Confocal images of GFP expression in

bioRxiv preprint doi: https://doi.org/10.1101/2021.02.16.431453; this version posted February 17, 2021. The copyright holder for this preprint (which was not certified by peer review) is the author/funder, who has granted bioRxiv a license to display the preprint in perpetuity. It is made available under aCC-BY 4.0 International license.

873 *Col6a1*^{mTmG} and *Col6a1*^{DTR} mice (Scale bar = 50 μm). C) FACS analysis and
874 quantification of GFP^{+} cells in the colon of *Col6a1*^{mTmG} and *Col6a1*^{DTR} mice after DT
875 administration (n = 9). D) FACS analysis and quantification of PDGFRα^{+} subsets in
876 GFP^{+} cells in *Col6a1*^{mTmG} and *Col6a1*^{DTR} mice (n = 3-5). E) FACS analysis and
877 quantification of CD201^{+}PDGFRα^{hi} cells in *Col6a1*^{mTmG} and *Col6a1*^{DTR} mice (n = 3-4
878 mice). F) FACS analysis of PDGFRα^{+} subsets in *Col6a1*^{mTmG} and *Col6a1*^{DTR} mice (n
879 = 4-10). G) H&E staining of *Col6a1*^{DTR} and control (*Col6a1*^{mTmG}, *iDTR*$^{f/f/}$) mice
880 (Scale bar: 100 μm). H) Expression analysis of the indicated genes in colon samples
881 from *Col6a1*^{DTR} and control (*Col6a1*^{mTmG}, *iDTR*$^{f/f/}$) mice. Expression is measured in
882 relation to the *B2m* housekeeping gene (n = 9-14). I)_Immunohistochemical-based
883 quantification of differentiated epithelial cell types per crypt in *Col6a1*^{DTR} and control
884 (*Col6a1*^{mTmG}, *iDTR*$^{f/f/}$) mice (n = 5-13). J) Expression analysis of the indicated genes
885 in colon samples from *Col6a1*^{DTR} and control (*Col6a1*^{mTmG}, *iDTR*$^{f/f/}$) mice. Expression
886 is measured in relation to the *B2m* housekeeping gene (n = 5-15). K) Representative
887 BrdU staining and L) quantification of the ratio of BrdU^{+} cells in the top/bottom of
888 the colonic crypts of *Col6a1*^{DTR} and control (*Col6a1*^{mTmG}, *iDTR*$^{f/f/}$) mice (Scale bar:
889 100 μm), (n = 6-7). *p<0.05, **p<0.01, ***p<0.001.
890

891 **Figure 5. CD34^{+} mesenchymal cells compensate for the loss of *Col6a1*$^{Cre+}$ cells.** A)
892 Immunohistochemical and B) FACS analysis of CD34 and PDGFRα expression in the
893 colon of *Col6a1*^{DTR} and *Col6a1*^{mTmG} mice (Scale bar = 50 μm) (n = 6 mice). A
894 zoomed-in view of the crypt top is shown in the merged image. C)
895 Immunohistochemical analysis and D) quantification of Ki67^{+} mesenchymal cells in
896 the colon of *Col6a1*^{DTR} and *Col6a1*^{mTmG} mice (Scale bar = 50 μm) (n = 5 mice). Both
897 broad and zoomed-in views of the crypt top are shown. E) Immunohistochemical

bioRxiv preprint doi: https://doi.org/10.1101/2021.02.16.431453; this version posted February 17, 2021. The copyright holder for this preprint (which was not certified by peer review) is the author/funder, who has granted bioRxiv a license to display the preprint in perpetuity. It is made available under aCC-BY 4.0 International license.

898 analysis of αSMA expression in the colon of *Col6a1^DTR^* and control mice (the top of
899 the crypt is shown) (n = 5). F) FACS analysis and G) quantification of αSMA^+ cells in
900 the $CD34^+$ subset (n = 4 mice), ***p<0.001.

901

902 **Figure 6. *Col6a1*$^{Cre+}$ cells retain their properties and topology during colitis but**
903 **are dispensable for tissue regeneration.** A) FACS sorting strategy for the isolation
904 of *Col6a1*^{Cre}-GFP^+ (GDS) and *Col6a1*^{Cre}-GFP^- (TDS) mesenchymal cells from the
905 colon at the end of the acute DSS protocol. 3 samples from 4-5 mice each were
906 subsequently analyzed. B) Heatmap of differentially expressed genes in GDS vs TDS
907 and UDS, as well as the respective untreated samples, corresponding to GO terms
908 related to epithelial proliferation/differentiation, blood vessel regulation and
909 inflammatory response. Log2 transformed normalized read counts of genes are
910 shown. Read counts are scaled per column, red denotes high expression and blue low
911 expression values. C) Confocal images of GFP expression in *Col6a1*^{mTmG} mice at day
912 8 of the acute DSS protocol, Scale bar = 50 μm. D) Mean expression (z-score) of
913 genes signatures extracted from the different intestinal mesenchymal clusters
914 identified in Kinchen et al., (14) during DSS colitis in *Col6a1*-GFP^+ bulk RNA-seq
915 samples. MF, myofibroblasts. E) Schematic representation of DT administration
916 during acute colitis and regeneration. Mice received 2.5% DSS for 5 days, followed
917 by regular water for 16 days. 100μl DT (*20ng/g* body weight) was administered
918 intrarectally at days 4, 5 and 6 of the regime. F) Quantification of GFP^+ cells in the
919 colon of control and *Col6a1*^{DTR} mice after DT administration (n = 5-7 mice), G) H&E
920 staining and H) histopathological score of *Col6a1*^{DTR} and control (*Col6a1*^{mTmG},
921 *iDTR*$^{f/f/}$) mice at the end of the protocol (Scale bar = 100 μm) (n = 10-11 mice).
922 Immunohistochemical analysis of I) CD34 and PDGFRα expression and J) CD34 and

bioRxiv preprint doi: https://doi.org/10.1101/2021.02.16.431453; this version posted February 17, 2021. The copyright holder for this preprint (which was not certified by peer review) is the author/funder, who has granted bioRxiv a license to display the preprint in perpetuity. It is made available under aCC-BY 4.0 International license.

923 αSMA expression in the colon of *Col6a1*^{DTR} and control mice (Scale bar = 50 μm) (n

924 = 4 mice).

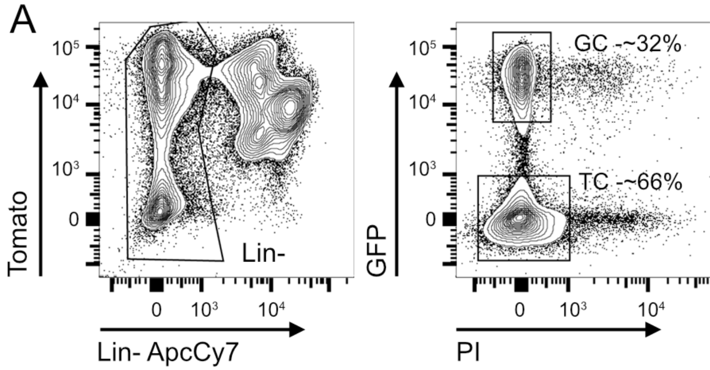
A
Tomato
Lin-
Lin- ApcCy7
GFP
GC ~32%
TC ~66%
PI

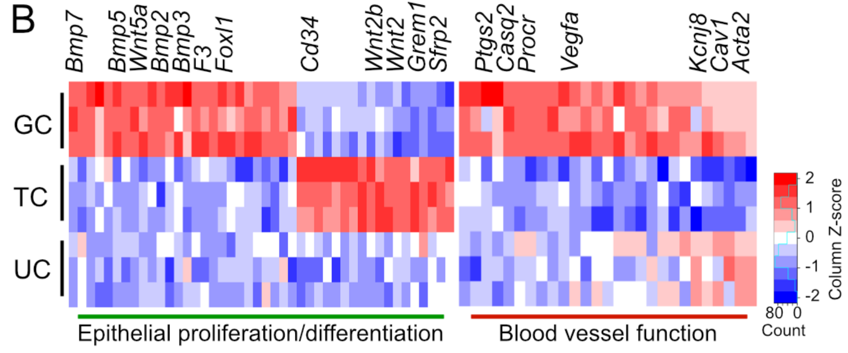
B
Bmp7
Bmp5
Wnt5a
Bmp2
Bmp3
F3
Foxl1
Cd34
Wnt2b
Wnt2
Grem1
Sfrp2
Ptgs2
Casq2
Procr
Vegfa
Kcnj8
Cav1
Acta2
GC
TC
UC
Epithelial proliferation/differentiation
Blood vessel function
Column Z-score
Count

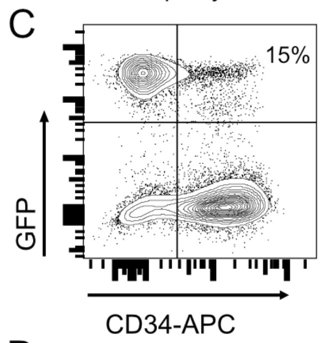
C
15%
GFP
CD34-APC

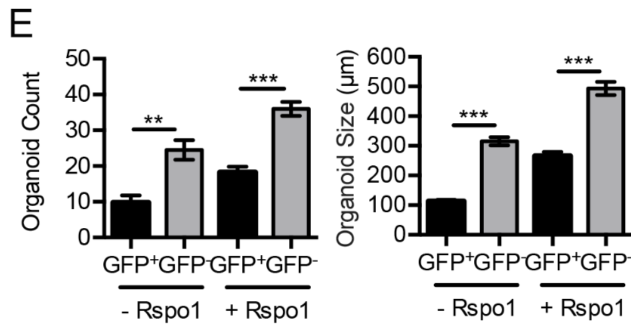
E
Organoid Count
Organoid Size (μm)
GFP+ GFP- GFP+ GFP-
- Rspo1
+ Rspo1

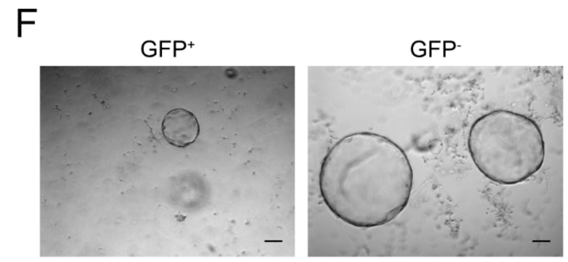
F
GFP+
GFP-

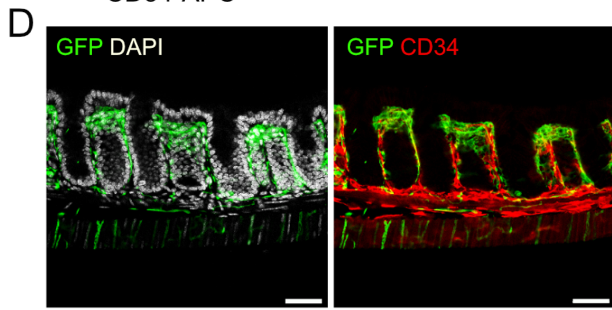
D
GFP DAPI
GFP CD34

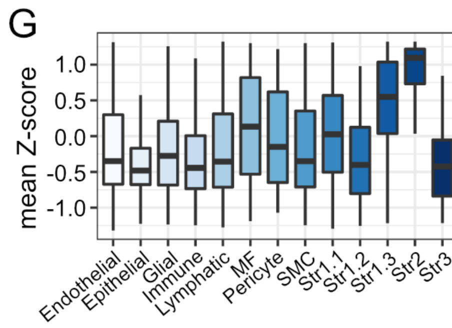
G
mean Z-score
Endothelial
Epithelial
Glial
Immune
Lymphatic
MF
Pericyte
SMC
Str1.1
Str1.2
Str1.3
Str2
Str3

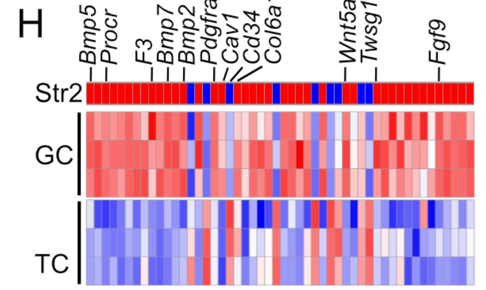
H
Bmp5
Procr
F3
Bmp7
Bmp2
Pdgfra
Cav1
Cd34
Col6a1
Wnt5a
Twsg1
Fgf9
Str2
GC
TC

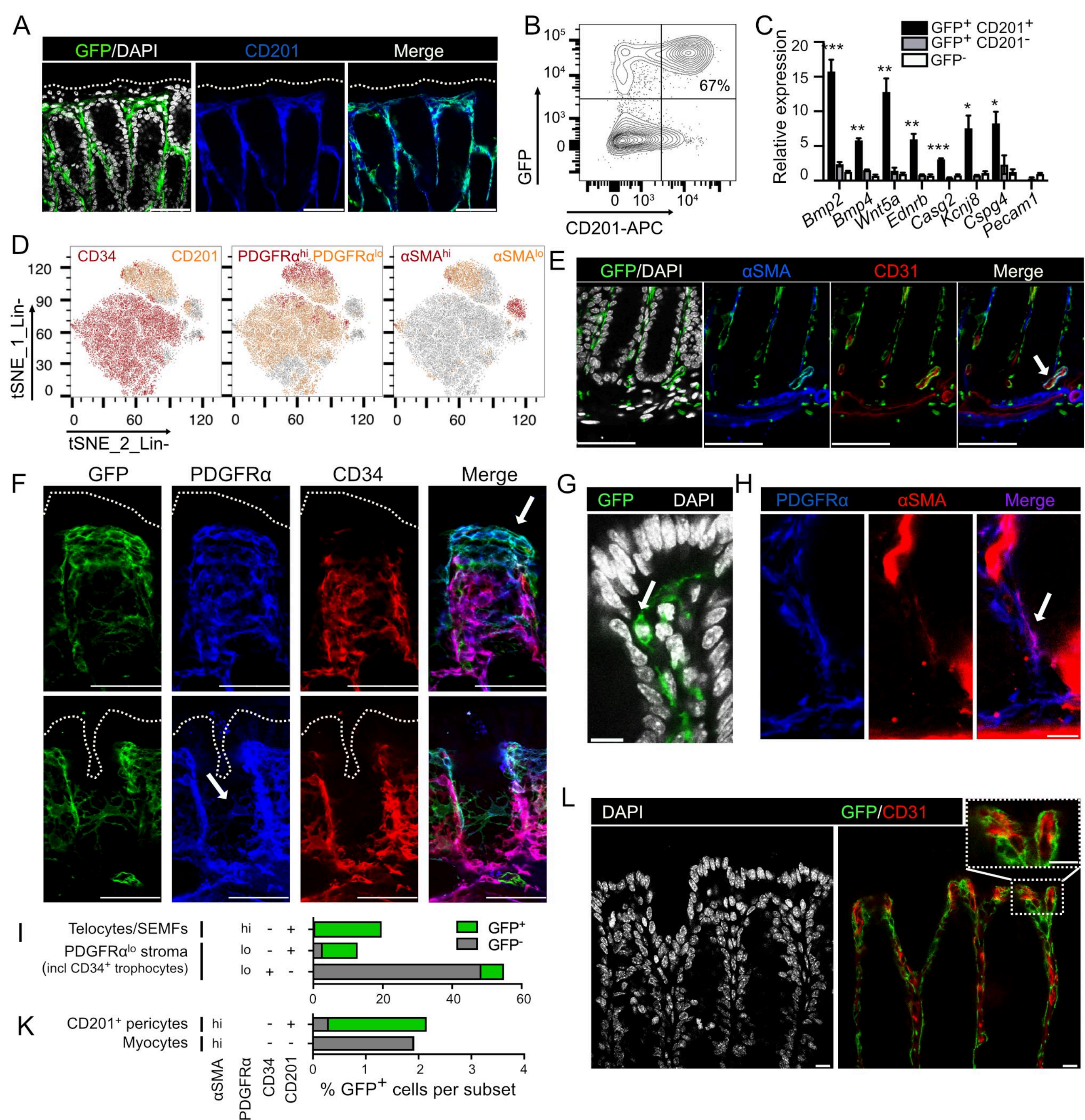

A
GFP/DAPI
CD201
Merge
B
GFP
CD201-APC
67%
C
Relative expression
GFP+ CD201+
GFP+ CD201-
GFP-
Bmp2
Bmp4
Wnt5a
Ednrb
Casq2
Kcnj8
Cspg4
Pecam1
D
CD34
CD201
PDGFRαhi
PDGFRαlo
αSMAhi
αSMAlo
tSNE_1_Lin-
tSNE_2_Lin-
E
GFP/DAPI
αSMA
CD31
Merge
F
GFP
PDGFRα
CD34
Merge
G
GFP
DAPI
H
PDGFRα
αSMA
Merge
I
Telocytes/SEMFs
PDGFRαlo stroma
(incl CD34+ trophocytes)
GFP+
GFP-
K
CD201+ pericytes
Myocytes
αSMA
PDGFRα
CD34
CD201
% GFP+ cells per subset
L
DAPI
GFP/CD31

A
Small intestine
Colon
GFP/DAPI
PDGFRα
GFP/PDGFRα
Merge-zoomed

B
GFP/Tomato
PDGFRα
GFP/PDGFRα
Zoomed
Small Intestine
Colon
E18.5
P4
E18.5
P3

C
GFP/Tomato/αSMA
Small Intestine
Colon
E15.5
E18.5
E15.5
E18.5

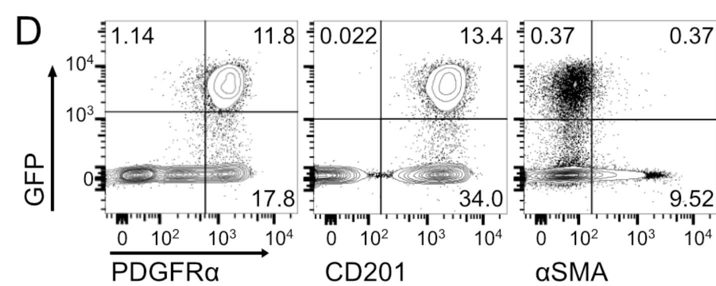

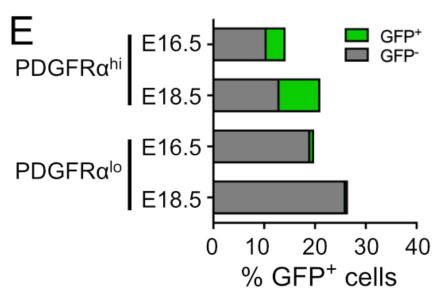

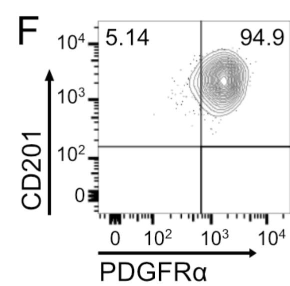

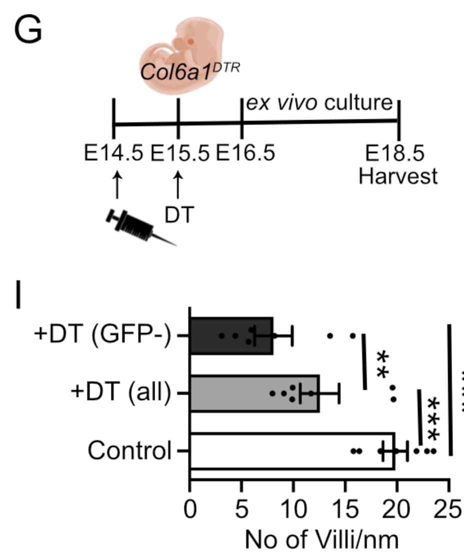

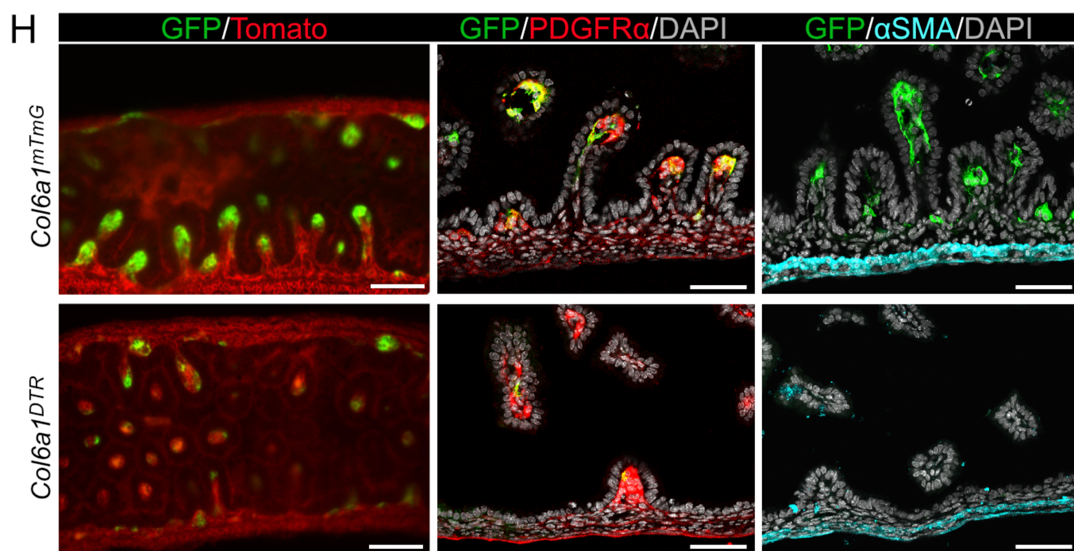

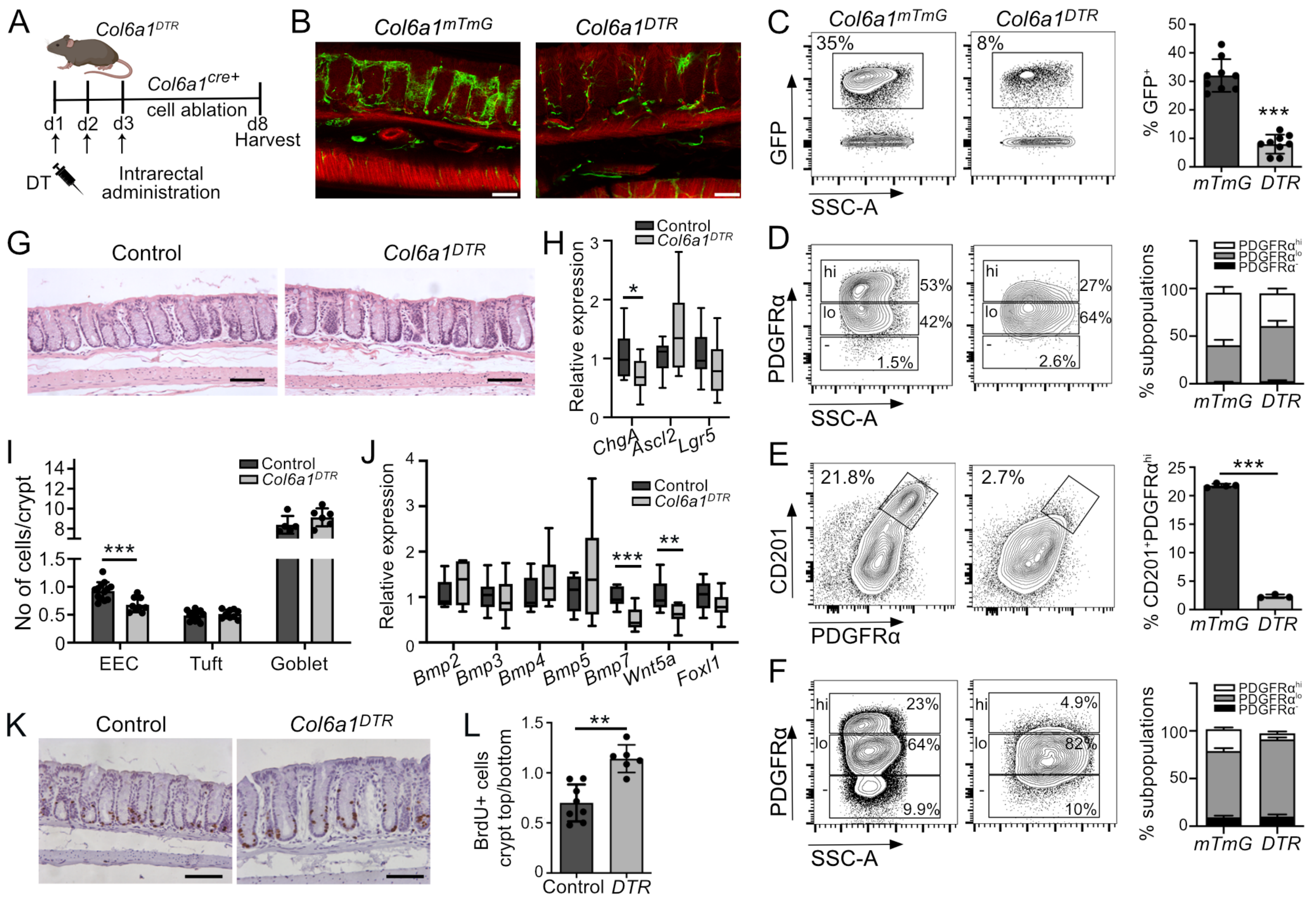
A
Col6a1DTR
Col6a1cre+
cell ablation
d1 d2 d3 d8
Harvest
DT
Intrarectal administration
B
Col6a1mTmG
Col6a1DTR
C
35%
8%
GFP
SSC-A
% GFP+
mTmG DTR
***
D
PDGFRα
hi lo -
53% 42% 1.5%
27% 64% 2.6%
% subpopulations
PDGFRαhi PDGFRαlo PDGFRα-
E
CD201
PDGFRα
21.8%
2.7%
% CD201+PDGFRαhi
F
23% 64% 9.9%
4.9% 82% 10%
G
Control
Col6a1DTR
H
Relative expression
Control
Col6a1DTR
ChgA Ascl2 Lgr5
I
No of cells/crypt
EEC Tuft Goblet
J
Bmp2 Bmp3 Bmp4 Bmp5 Bmp7 Wnt5a Foxl1
K
L
BrdU+ cells crypt top/bottom
Control DTR
**

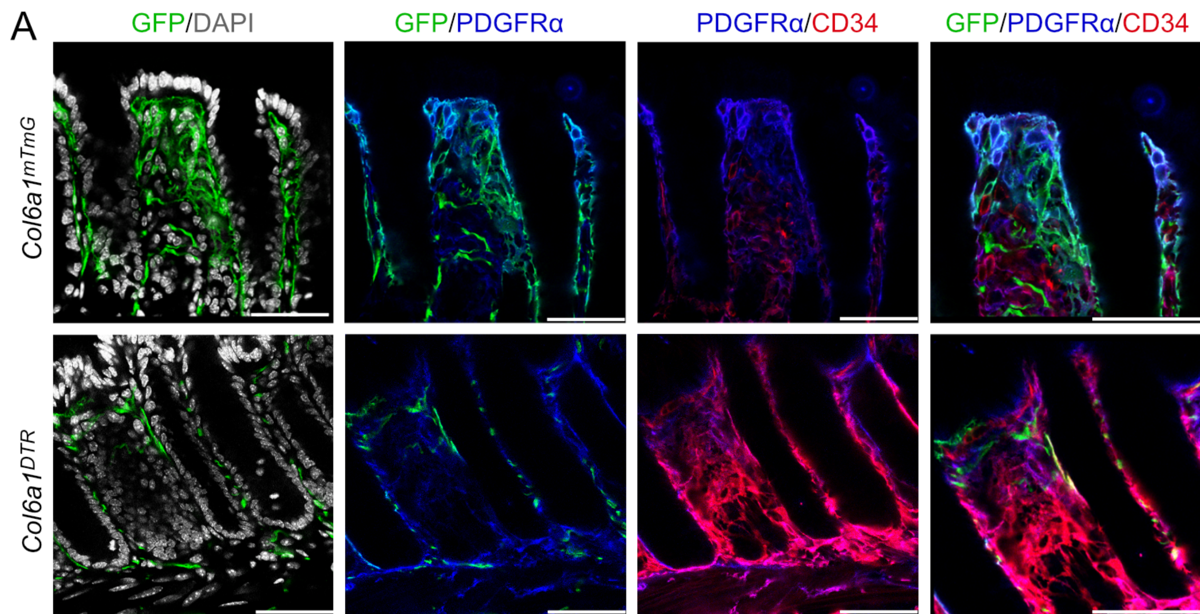
A
GFP/DAPI
GFP/PDGFRα
PDGFRα/CD34
GFP/PDGFRα/CD34
Col6a1mTmG
Col6a1DTR

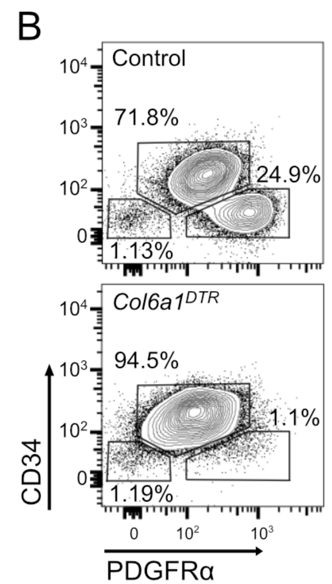
B
Control
71.8%
24.9%
1.13%
Col6a1DTR
94.5%
1.1%
1.19%
CD34
PDGFRα

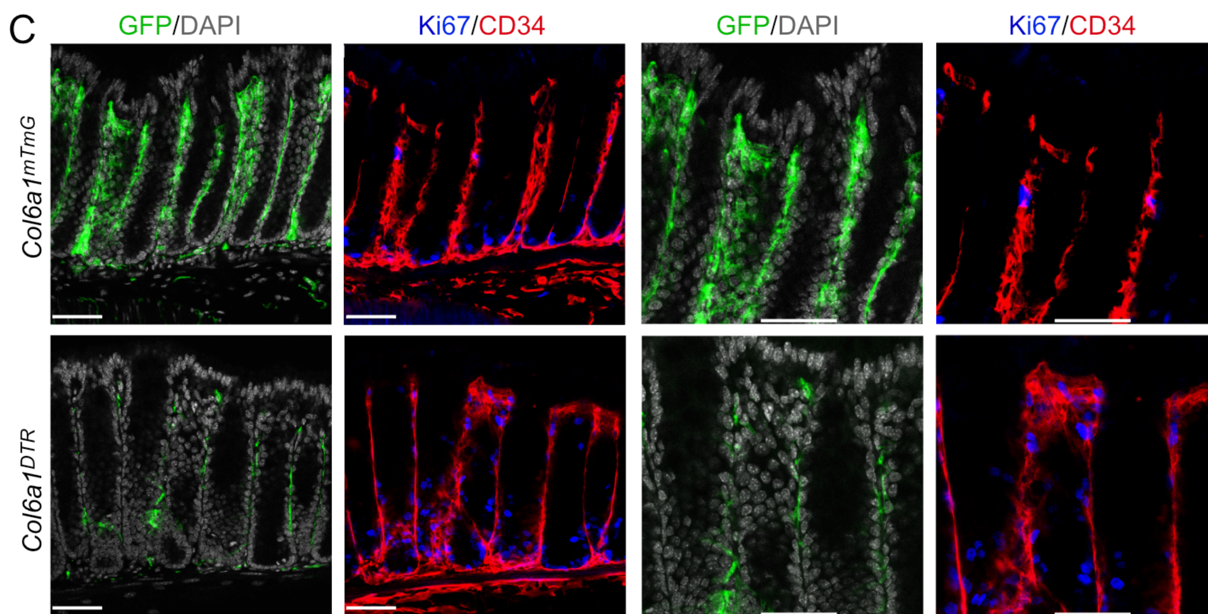
C
GFP/DAPI
Ki67/CD34
GFP/DAPI
Ki67/CD34
Col6a1mTmG
Col6a1DTR

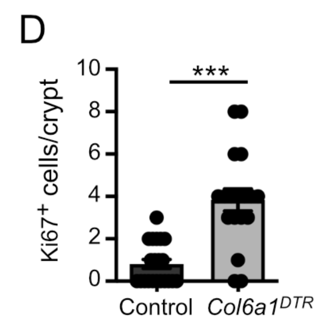
D
Ki67+ cells/crypt
***
Control
Col6a1DTR

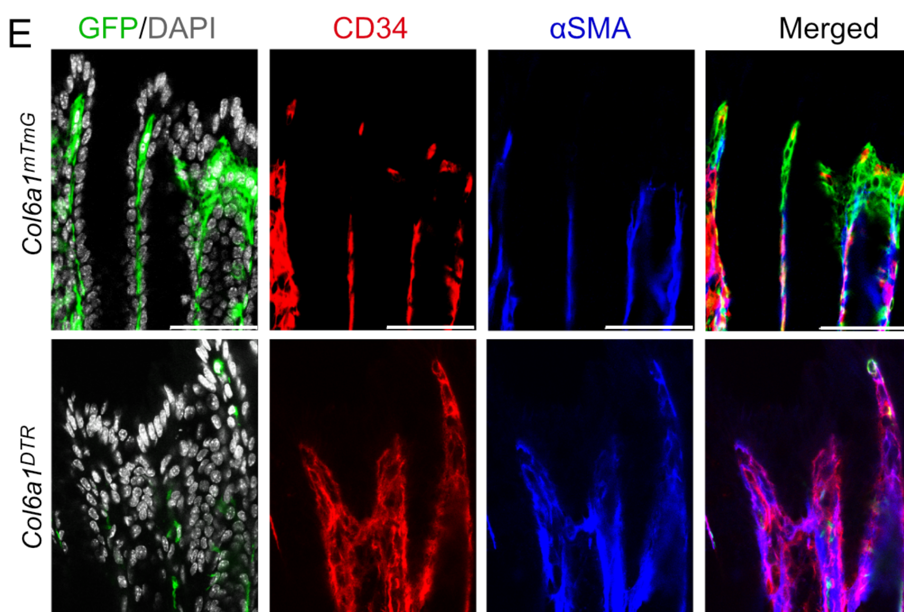
E
GFP/DAPI
CD34
αSMA
Merged
Col6a1mTmG
Col6a1DTR

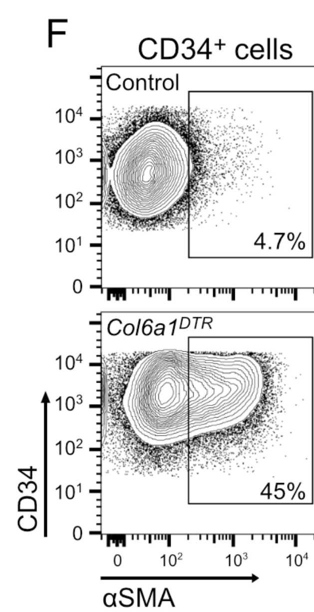
F
CD34+ cells
Control
4.7%
Col6a1DTR
45%
CD34
αSMA

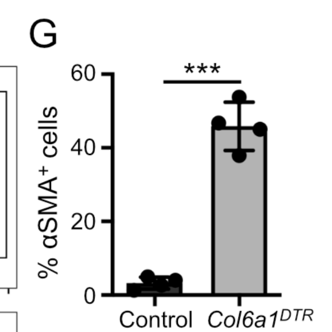
G
% αSMA+ cells
***
Control
Col6a1DTR

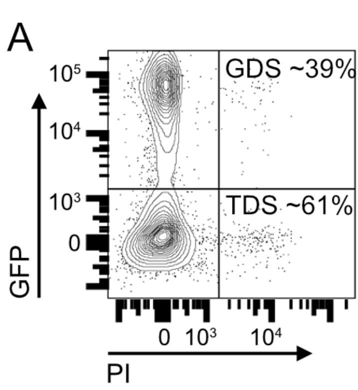
A
GDS ~39%
TDS ~61%
GFP
PI

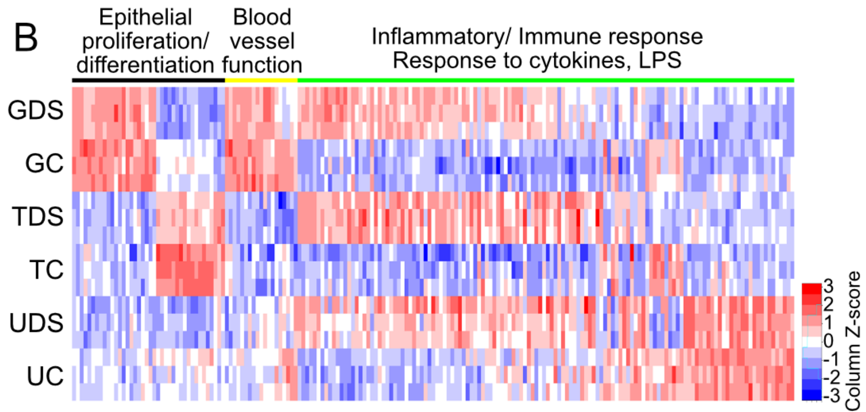
B
Epithelial proliferation/ differentiation
Blood vessel function
Inflammatory/ Immune response
Response to cytokines, LPS
GDS
GC
TDS
TC
UDS
UC
Column Z-score

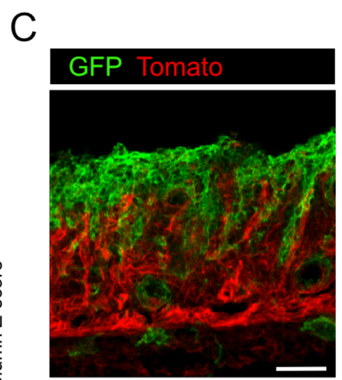
C
GFP Tomato

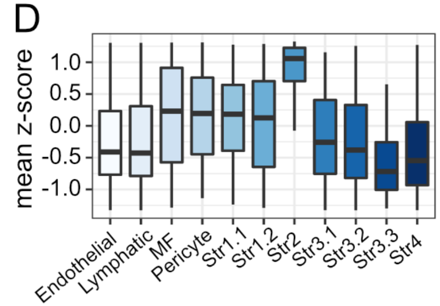
D
mean z-score
Endothelial
Lymphatic
MF
Pericyte
Str1.1
Str1.2
Str2
Str3.1
Str3.2
Str3.3
Str4

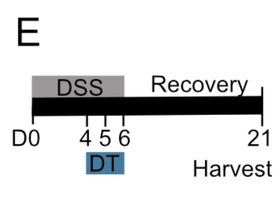
E
DSS
Recovery
D0
4 5 6
21
DT
Harvest

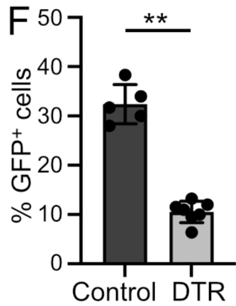
F
% GFP⁺ cells
**
Control
DTR

G
Control
Col6a1DTR

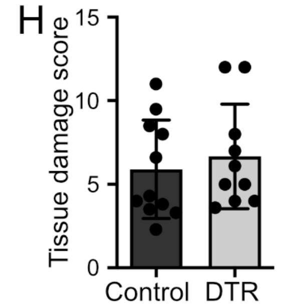
H
Tissue damage score
Control
DTR

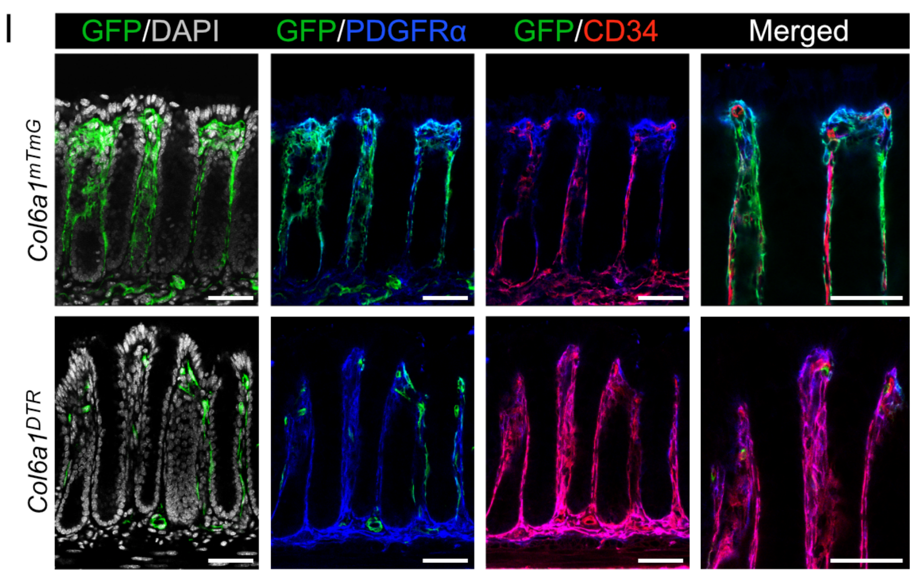
I
GFP/DAPI
GFP/PDGFRα
GFP/CD34
Merged
Col6a1mTmG
Col6a1DTR

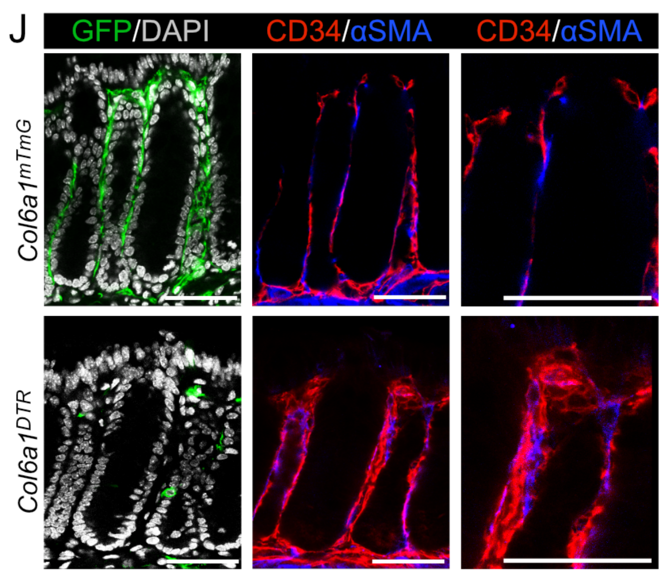
J
GFP/DAPI
CD34/αSMA
CD34/αSMA
Col6a1mTmG
Col6a1DTR